Loss of ZNRF3/RNF43 Unleashes EGFR in Cancer

Fei Yue[1,2*], Amy T. Ku[1], Payton D. Stevens[3], Megan N. Michalski[3], Weiyu Jiang[1], Jianghua Tu[4], Zhongcheng Shi[5], Yongchao Dou[1], Yi Wang[6], Xin-Hua Feng[7], Galen Hostetter[8], Xiangwei Wu[9], Shixia Huang[5,10,11,12], Noah F. Shroyer[2,12], Bing Zhang[1,12,13], Bart O. Williams[3,8], Qingyun Liu[4], Xia Lin[14], Yi Li[1,10,12,15*]

[1]Lester and Sue Smith Breast Center, Baylor College of Medicine, Houston, Texas 77030, USA.
[2]Department of Medicine, Baylor College of Medicine, Houston, Texas 77030, USA.
[3]Van Andel Institute, Department of Cell Biology, Grand Rapids, Michigan, 49503, USA.
[4]Texas Therapeutics Institute and Brown Foundation Institute of Molecular Medicine, University of Texas Health Science Center at Houston, Houston, Texas 77030, USA.
[5]Advanced Technology Cores, Baylor College of Medicine, Houston, Texas 77030, USA.
[6]State Key Laboratory of Proteomics, Beijing Proteome Research Center, National Center for Protein Sciences (Beijing), Beijing Institute of Lifeomics, Beijing 102206, China.
[7]Life Sciences Institute, Zhejiang University, Hangzhou, Zhejiang 310058, China.
[8]Van Andel Institute, Core Technologies and Services, Grand Rapids, Michigan 49503, USA.
[9]Department of Clinical Cancer Prevention, The University of Texas MD Anderson Cancer Center, Houston, Texas 77030, USA.
[10]Department of Molecular and Cellular Biology, Baylor College of Medicine, Houston, Texas 77030, USA.
[11]Department of Education, Innovation & Technology, Baylor College of Medicine, Houston, Texas 77030, USA.
[12]Dan L. Duncan Comprehensive Cancer Center, Baylor College of Medicine, Houston, Texas 77030, USA.
[13]Department of Molecular and Human Genetics, Baylor College of Medicine, Houston, Texas 77030, USA.
[14]The First Affiliated Hospital of Zhejiang University, Hangzhou, Zhejiang 310003, China.
[15]Department of Molecular Virology and Microbiology, Baylor College of Medicine, Houston, Texas 77030, USA.
*Correspondence: fyue@bcm.edu; liyi@bcm.edu

Keywords

Cell signaling | Cancer | Ubiquitination | EGFR

Abstract

ZNRF3 and RNF43 are closely related transmembrane E3 ubiquitin ligases with significant roles in development and cancer. Conventionally, their biological functions have been associated with regulating WNT signaling receptor ubiquitination and degradation. However, our proteogenomic studies have revealed EGFR as the most negatively correlated protein with *ZNRF3/RNF43* mRNA levels in multiple human cancers. Through biochemical investigations, we demonstrate that ZNRF3/RNF43 interact with EGFR via their extracellular domains, leading to EGFR ubiquitination and subsequent degradation facilitated by the E3 ligase RING domain. Overexpression of *ZNRF3* reduces EGFR levels and suppresses cancer cell growth *in vitro* and *in vivo*, whereas knockout of *ZNRF3*/*RNF43* stimulates cell growth and tumorigenesis through upregulated EGFR signaling. Together, these data highlight ZNRF3 and RNF43 as novel E3 ubiquitin ligases of EGFR and establish the inactivation of ZNRF3/RNF43 as a driver of increased EGFR signaling, ultimately promoting cancer progression. This discovery establishes a connection between two fundamental signaling pathways, EGFR and WNT, at the level of cytoplasmic membrane receptor, uncovering a novel mechanism underlying the frequent co-activation of EGFR and WNT signaling in development and cancer.

53 **Introduction**

54 Zinc And Ring Finger 3 (ZNRF3) and Ring Finger Protein 43 (RNF43) are two closely related
55 single-pass transmembrane E3 ligases with significant roles in embryonic development, tissue
56 homeostasis and regeneration, and diseases (Basham *et al*, 2019; Hao *et al*, 2012; Koo *et al*, 2012;
57 Lee *et al*, 2020; Planas-Paz *et al*, 2016; Sun *et al*, 2021; Szenker-Ravi *et al*, 2018). Extensive
58 research has demonstrated their involvement in critical processes such as limb development
59 (Szenker-Ravi *et al.*, 2018), liver zonation (Planas-Paz *et al.*, 2016), and mammalian sex
60 determination (Harris *et al*, 2018). These two enzymes also function as tumor suppressors, as
61 evidenced by the promotion of intestinal and adrenal hyperplasia (Basham *et al.*, 2019; Koo *et al.*,
62 2012) and hepatocellular carcinogenesis (Mastrogiovanni *et al*, 2020) upon tissue-specific
63 inactivation of *Znrf3*/*Rnf43.* Similarly, *Rnf43* deficiency leads to thickened mucosa, hyperplasia
64 and cellular atypia in the stomach (Neumeyer *et al*, 2019), and enhanced tumor growth in a mouse
65 model of inflammatory colorectal cancer (Eto *et al*, 2018). Conversely, overexpression of ZNRF3
66 and RNF43 suppresses cancer cell proliferation, migration and invasion, and drug resistance in
67 multiple human cancer cell lines (Jiang *et al*, 2013; Pangestu *et al*, 2021; Qiu *et al*, 2016;
68 Radaszkiewicz *et al*, 2021; Zhou *et al*, 2013). Importantly, in cancer patients, ZNRF3 and RNF43
69 are frequently inactivated by gene deletion or loss-of-function mutations (Hao *et al*, 2016; Yu *et*
70 *al*, 2020). For instance, *ZNRF3* is the most altered gene in adrenocortical carcinomas (ACCs),
71 homozygously deleted in approximately 20% of ACCs (Assie *et al*, 2014). *RNF43* is mutated in
72 approximately 15% of endometrial cancer, 12% of stomach cancer, 11% of colorectal cancer, and
73 7% of pancreatic cancer (Tu *et al*, 2019). These findings highlight the clinical significance of
74 ZNRF3/RNF43 and the importance of fully understanding the molecular mechanism(s) by which
75 they affect development and cancer.

76

77 The primary known molecular function of ZNRF3/RNF43 is the regulation of WNT signaling. As
78 transmembrane E3 ligases, they ubiquitinate the WNT signaling receptor Frizzled, targeting it for
79 degradation thus dampening WNT signaling (Hao *et al.*, 2012; Koo *et al.*, 2012). Conversely, R-
80 spondins (RSPO1-4) act as antagonistic peptide ligands, binding to ZNRF3/RNF43 and promoting
81 their auto-ubiquitination and membrane clearance, thus maintaining WNT receptor levels and
82 potentiating WNT signaling (Carmon *et al*, 2011; de Lau *et al*, 2011; Dubey *et al*, 2020; Glinka *et*
83 *al*, 2011; Hao *et al.*, 2012; Koo *et al.*, 2012; Lebensohn & Rohatgi, 2018; Park *et al*, 2018; Park *et*
84 *al*, 2020; Szenker-Ravi *et al.*, 2018). Furthermore, activation of WNT signaling transactivates
85 *ZNRF3* and *RNF43* expression via β-Catenin (Hao *et al.*, 2012; Koo *et al.*, 2012), creating a
86 negative feedback loop that tightly regulates WNT signaling during normal development and
87 tissue homeostasis. However, in cancer cells, alterations such as recurrent *RSPO* gene fusion or
88 *ZNRF3/RNF43* deletion or mutations disrupts this feedback loop, resulting in hyperactive WNT
89 signaling and subsequent cancer development and progression (Hao *et al.*, 2016; Seshagiri *et al*,
90 2012).

91

92 Although most molecular functions of RSPO-ZNRF3/RNF43 have been linked to their modulation
93 of WNT signaling, emerging evidence suggests that ZNRF3 and RNF43 may possess WNT-
94 independent functions. For instance, RSPO and WNT ligands exhibit non-equivalent roles in
95 various processes, including mammary epithelial cell growth (Klauzinska *et al*, 2012), mammary
96 side branches (Geng *et al*, 2020), intestinal stem cell self-renewal (Yan *et al*, 2017), and cochlea
97 development (Mulvaney *et al*, 2013). Furthermore, loss of RNF43 function promotes mouse
98 gastric epithelium proliferation and human gastric cancer cell xenograft growth, without detectable

99 impact on WNT signaling activity (Neumeyer *et al*, 2020; Neumeyer *et al.*, 2019). Additionally,
100 the inhibitory effects of RSPO-ZNRF3 on BMP signaling are not abolished by *β-Catenin*
101 knockdown (Lee *et al.*, 2020). Moreover, approximately 40% of *ZNRF3* or *RNF43*-mutant colon
102 tumors also harbor alterations in either *APC* or *CTNNB1*, suggesting the involvement of these E3
103 ligases beyond the regulation of WNT signaling (Cerami *et al*, 2012; Gao *et al*, 2013). This is
104 further supported by a recent report of a hotspot *RNF43* G659 frameshift mutation that does not
105 appear to affect WNT signaling (Fang *et al*, 2022). However, the extent to which ZNRF3 and
106 RNF43 act on other substrates, apart from WNT receptors, to influence development and cancer
107 has been unclear.
108
109 In this study, we report a new function of ZNRF3 and RNF43. Initially, we observed a strong
110 negative correlation between *ZNRF3/RNF43* mRNA levels and EGFR protein expression in
111 datasets of human adrenocortical carcinomas and colorectal cancers. Subsequently, we
112 investigated the impact of depleting *ZNRF3* or *RNF43* on EGFR clearance at the cell surface in
113 mouse embryonic fibroblasts (MEFs) and human cancer cell lines including *APC*-mutated
114 colorectal cancer cells. Notably, we discovered that ZNRF3/RNF43 interact with EGFR through
115 their extracellular domains, leading to EGFR ubiquitination and degradation via the E3 ligase
116 RING domain. Additionally, we substantiated our findings in multiple cell lines, human cancer
117 cell xenograft models, and genetically engineered mouse models, wherein the loss of
118 *ZNRF3*/*RNF43* resulted in elevated EGFR levels and facilitated cancer progression.
119
120 **Results**

121 **EGFR protein levels negatively correlate with *ZNRF3/RNF43* mRNA expression in multiple**
122 **human cancers**

123 To elucidate novel signaling pathways regulated by ZNRF3/RNF43 in cancer, we conducted
124 integrative proteogenomic analyses of human cancer datasets using LinkedOmics (Vasaikar *et al*,
125 2018). Given the critical role of *ZNRF3* in adrenal hemostasis (Basham *et al.*, 2019) and its
126 frequent deep deletion in approximately 20% of adrenocortical carcinomas (ACCs) (Assie *et al.*,
127 2014), our initial focus was to examine the ACC dataset from TCGA, comprising 92 samples, to
128 identify proteins exhibiting correlations with *ZNRF3* mRNA levels. Among the proteins evaluated
129 by Reverse Phase Protein Array (RPPA), our analysis revealed EGFR protein levels to be most
130 negatively correlated with *ZNRF3* mRNA levels (r = -0.50 and p = 4.5e-4) (Fig. 1A and Fig. S1A).
131 Notably, ACC tumors with deep deletion in *ZNRF3* exhibited highest EGFR protein levels
132 compared to ACC tumors with other alterations in the *ZNRF3* locus (Fig. 1B). These findings
133 suggest that disruption of the gene function of *ZNRF3* may lead to upregulation of EGFR in ACCs.
134

135 Besides frequent deletions in ACC, *ZNRF3* and *RNF43* are also important tumor suppressors in
136 the more commonly occurring colorectal cancer (CRC) (Bond *et al*, 2016; Koo *et al.*, 2012); thus,
137 we next analyzed the TCGA colorectal adenocarcinoma (n=629) and CPTAC colon
138 adenocarcinoma (n=210) datasets. By incorporating RPPA-based (TCGA CO/READ) and mass
139 spectrometry-based (CPTAC COAD) proteomic data, we confirmed EGFR protein also to be the
140 one most negatively correlated with *ZNRF3* and *RNF43* mRNA expression in CRC (Fig. 1C and
141 Fig. S1B-E). Of note, we utilized mRNA abundance of *ZNRF3/RNF43* mRNA abundances rather
142 than protein levels due to the lack of protein measurements for these two low-abundance enzymes
143 in the current proteomic datasets. Mutations in *ZNRF3/RNF43* are found in approximately 15% of

144 CRCs overall, with high frequencies observed in the microsatellite instability-high (MSI-H)
145 subtype (60%-80%) (Bond *et al.*, 2016; Giannakis *et al*, 2014; Tu *et al.*, 2019; Vasaikar *et al*,
146 2019). In particular, the *RNF43* G659Vfs*41 frameshift mutation accounts for 40-50% of all
147 *RNF43* mutations in multiple MSI-H cancer types (Tu *et al.*, 2019). Interestingly, CRCs harboring
148 the *RNF43* G659Vfs*41 mutation exhibited significantly higher levels of EGFR protein compared
149 to *RNF43* wild-type (WT) tumors (Fig. 1D and Fig. S1F). A similar difference was observed in
150 stomach cancer, which also displayed a high frequency of the *RNF43* G659Vfs*41 mutation (Fig.
151 S1G). Additionally, in the microsatellite stable (MSS) subtype of CRCs, predominantly expressing
152 WT RNF43, we found a negative association between *RNF43* mRNA and EGFR protein levels
153 (r=-0.36 and p=0.0018) (Fig. 1E). Using cBioPortal (Cerami *et al.*, 2012; Gao *et al.*, 2013), we
154 also detected a negative correlation between *ZNRF3/RNF43* expression and EGFR protein in
155 multiple other cancer types, including prostate cancer where *ZNRF3* or *RNF43* is deleted or
156 mutated with a rate of 5% (Fig. 1F). Collectively, these results suggest that disruption of *ZNRF3*
157 and *RNF43* may up-regulate EGFR protein levels in human cancers.
158

159 **ZNRF3 and RNF43 downregulate the EGFR protein level**

160 To test whether ZNRF3 and RNF43 regulate EGFR protein, we performed gain-of-function and
161 loss-of-function experiments in several cell lines. In MDA-MB-231, a breast cancer cell line with
162 intermediate levels of ZNRF3/RNF43, overexpression of either ZNRF3 or RNF43 substantially
163 reduced EGFR protein levels (Fig. 2A). Remarkably, ZNRF3 and RNF43 decreased EGFR as
164 robustly as CBL, the best-known E3 ligase of EGFR (Levkowitz *et al*, 1998; Waterman *et al*,
165 1999). Similarly, in 293T cells, ZNRF3/RNF43 overexpression reduced the levels of EGFR (Fig.
166 S2A). As predicted, the phosphorylated form of EGFR declined as well (Fig. S2A). Notably, the

167 reduction in both total EGFR and P-EGFR levels reached an extent comparable to that achieved
168 by CBL (Fig. S2A). Consistent with their known function, ZNRF3/RNF43 overexpression reduced
169 the level of their substrate FZD5 (Hao *et al.*, 2012; Koo *et al.*, 2012) (Fig. S2A). Additionally,
170 these two E3 ligases exhibited selectivity in their regulation of growth factor receptors since
171 overexpression of ZNRF3 or RNF43 did not decrease levels of TGFβ receptor-I (Fig. S2B) or
172 FGFR1 (Fig. S2C).
173
174 To test the impact of *ZNRF3/RNF43* loss on EGFR levels, we compared WT and *Znrf3* knockout
175 (KO) MEFs because the WT MEFs have adequate *Znrf3* expression but very minimal *Rnf43*
176 expression (Lienert *et al*, 2011). We found that *Znrf3* KO enhanced both EGFR and P-EGFR levels,
177 both in the absence and presence of recombinant EGF (Fig. 2B). To test the effect of *RNF43* KO,
178 we utilized HT29, a colorectal cancer cell line that expresses WT *RNF43* at a high level but
179 minimal *ZNRF3*. CRISPR-KO of *RNF43* enhanced EGFR and P-EGFR levels regardless of EGF
180 stimulation (Fig. 2C). We validated these results using three additional independent *RNF43*
181 gRNAs (Fig. S2D) and extended our analysis to HCC1954, a breast cancer cell line (Fig. S2E).
182 Since this line expresses the EGFR family member HER2, we also assayed the effects of *RNF43*
183 KO on HER2. We found that knockout of either *ZNRF3* or *RNF43* enhanced the protein levels of
184 HER2 (Fig. S2E), suggesting that ZNRF3 and RNF43 downregulate the levels of EGFR and its
185 family members and that the loss of these E3 ligases unleashes this family of receptor tyrosine
186 kinases.
187
188 RSPO1-4 are the antagonistic ligands of ZNRF3 and RNF43 (Hao *et al.*, 2012; Koo *et al.*, 2012).
189 They bind to both ZNRF3/RNF43 and LGR4/5/6, resulting in ZNRF3/RNF43 auto-ubiquitination

190 and degradation (Hao *et al.*, 2012; Koo *et al.*, 2012). Approximately 18% of CRCs harbor
191 amplification or mutations of *RSPO1-4* or *LGR4/5/6,* and 10% of CRCs show recurrent *RSPO2/3*
192 gene fusions (Seeber *et al*, 2019; Seshagiri *et al.*, 2012). These genetic alterations potentially lead
193 to the inhibition of ZNRF3/RNF43, thereby activating WNT and EGFR signaling. Therefore, we
194 tested whether RSPO affected EGFR protein levels in CRC. Short-term treatment with
195 recombinant RSPO2 increased EGFR levels in two CRC cell lines (Fig. 2D and E) as well as 293T
196 cells (Fig. S2F). Further, this impact of RSPO2 depended on the presence of intact ZNRF3/RNF43,
197 as RSPO2 failed to elevate EGFR levels in HT29 cells further knocked-out for *RNF43,* the
198 predominant one compared to *ZNRF3* (Fig. S2G). Conversely, the RSPO2 R65A/Q70A mutant,
199 which cannot bind to ZNRF3/RNF43 (Xie *et al*, 2013), failed to elevate EGFR levels (Fig. 2F).
200 On the other hand, the RSPO2 F105A/F109A mutant, which cannot bind to LGRs (Xie *et al.*,
201 2013), still enhanced EGFR levels similar to RSPO2 WT (Fig. 2E). These data collectively suggest
202 that RPSO2 regulation of EGFR does not rely on LGR-binding but requires its interaction with
203 ZNRF3/RNF43.
204
205 **ZNRF3 and RNF43 induce EGFR ubiquitination and degradation**
206 After demonstrating that ZNRF3 and RNF43 regulate EGFR protein levels, we next sought to
207 elucidate the underlying mechanism. We first examined whether ZNRF3 and RNF43 regulate
208 *EGFR* transcripts and found that ZNRF3/RNF43 did not impact *EGFR* mRNA levels in both MEFs
209 and HT29, as determined by qPCR (Fig. 3A and B). Then we studied the protein stability of EGFR
210 in WT and *RNF43* KO HT29 cells. We treated cells with recombinant EGF to induce EGFR
211 internalization/degradation and then collected cell lysates at different time points to measure
212 EGFR protein levels by Western blotting. We found that knockout of *RNF43* delayed EGFR
213 degradation and sustained P-EGFR levels (Fig. 3C). Since EGFR clearance is initiated at the cell

214 membrane and accelerated by EGF treatment, we also evaluated the impact of ZNRF3/RNF43 on
215 EGFR levels at the cell surface. Flow cytometry revealed that *ZNRF3* knockout in MEFs (Fig. 3D)
216 or *RNF43* knockout in HT29 (Fig. 3E) increased cell surface EGFR and inhibited EGF-induced
217 internalization of surface EGFR (indicated by the comparison of the black bar vs. red bar in Fig.
218 3D and E). These data together suggest that ZNRF3 and RNF43 induce cell surface EGFR
219 internalization and degradation.
220
221 EGFR degradation is primarily mediated by ubiquitination (Galcheva-Gargova *et al*, 1995;
222 Levkowitz *et al.*, 1998). To examine the impact of ZNRF3 and RNF43 on EGFR ubiquitination,
223 we performed EGFR immunoprecipitation (IP) followed by ubiquitin (Ub) immunoblotting (IB).
224 Remarkably, RNF43 overexpression in MDA-MB-231 cells enhanced EGFR ubiquitination as
225 potently as CBL overexpression (Fig. 4A). Conversely, in *RNF43* KO HT29 cells and MDA-MB-
226 231 cells, anti-Ubiquitin IP brought down substantially less EGFR protein (Fig. 4B and Fig. S3A),
227 and anti-EGFR IP produced much less ubiquitinated forms of EGFR (Fig. 4C), indicating that
228 *RNF43* knockout diminished EGFR ubiquitination. Next, we asked whether the E3 ligase activity
229 of ZNRF3/RNF43 is needed for regulating EGFR ubiquitination. The RING domain is required
230 for ZNRF3/RNF43 E3 ubiquitin ligase function (Pickart & Eddins, 2004). Therefore, we compared
231 the impact of ZNRF3/RNF43 vs. their RING domain deletion mutants (ΔRING) on EGFR protein
232 levels. We found that both ΔRING mutants failed to decrease EGFR levels (Fig. 4D and E) or
233 HER2 levels (Fig. S3B). Furthermore, while WT ZNRF3 overexpression increased EGFR
234 ubiquitination detectable even in the absence proteasome or lysosome inhibitors, the ΔRING
235 mutant failed to induce detectable upregulation of EGFR ubiquitination even in the presence of
236 both proteasome and lysosome inhibitors (MG132 and BAF, respectively) (Fig. 4F). Together,

237 these results demonstrate that ZNRF3 and RNF43 regulate EGFR ubiquitination and degradation
238 through their E3 ligase activity.
239
240 **ZNRF3 and RNF43 form a complex with EGFR through the extracellular domain**
241 We next investigated whether ZNRF3 and RNF43 interact with EGFR to regulate its ubiquitination.
242 In a co-IP experiment using lysates from MDA-MB-231 cells co-infected with lentivirus carrying
243 EGFR and Myc-tagged ZNRF3/RNF43, anti-EGFR IP pulled down overexpressed
244 ZNRF3/RNF43 (Fig. 5A), indicating a complex between EGFR and ZNRF3/RNF43. Mass
245 spectrometry of anti-EGFR immunoprecipitates identified endogenous ZNRF3 protein (Fig. S4A),
246 confirming ZNRF3 as an interacting partner of EGFR. Importantly, a proximity ligation assay
247 (PLA) provided visual confirmation of the close interaction between co-transfected ZNRF3 and
248 EGFR *in situ* (Fig. 5B). Next, we sought to determine the specific regions involved in the
249 interaction between ZNRF3/RNF43 and EGFR. ZNRF3 and RNF43 are transmembrane proteins
250 comprising a long extracellular domain (ECD), a single-span transmembrane domain (TM), and a
251 catalytic intracellular domain (ICD) (Fig. 5C). We thus generated constructs expressing ZNRF3
252 ECD-TM and TM-ICD, with an N-terminal 3X Myc-tag inserted after the signal peptide for
253 detection (Fig. 5C). Immunofluorescence (IF) confirmed the membrane localization of these two
254 peptides (Fig. 5D), after which we performed co-IP using anti-Myc. EGFR was co-
255 immunoprecipitated with Myc-tagged ZNRF3 full-length (FL) and ECD-TM, but not TM-ICD,
256 (Fig. 5E). Conversely, anti-EGFR IP pulled down ZNRF3 FL and ECD-TM, but not TM-ICD (Fig.
257 5E). Similar results were obtained when performing anti-HA IP of HA-tagged RNF43 FL and
258 ECD-TM, which also brought down EGFR (Fig. S4B and C). These data collectively indicate that
259 ZNRF3 and RNF43 interact with EGFR via their extracellular domains, in accordance with

260 evidence indicating the ZNRF3/RNF43 interaction with Frizzled via extracellular domains
261 (Tsukiyama *et al*, 2015). while in contrast with reports detecting ZNRF3/RN43 interaction with
262 Frizzled via their intracellular domains and other adaptor proteins (Jiang *et al*, 2015).
263
264 The protease-associated (PA) domain is the only conservative part between the extracellular
265 fragments of ZNRF3 and RNF43 (Tsukiyama *et al*, 2021). Therefore, we tested whether this
266 domain is necessary for the interaction between ZNRF3/RNF43 with EGFR. We created PA
267 domain-deletion mutants of ZNRF3/RNF43 (Fig. S5A) and found that these deletion mutants
268 (ΔPA) also interacted with EGFR (Fig. S5B and C), indicating that the PA domain is dispensable
269 for ZNRF3/RNF43 interaction with EGFR. In accordance with previous reports that the PA
270 domain is dispensable for suppression of WNT signaling (Jiang *et al.*, 2015; Radaszkiewicz &
271 Bryja, 2020), we found that ΔPA ZNRF3 retained the ability to suppress the Top-Flash WNT
272 reporter (Fig. S5D).
273
274 **Loss of ZNRF3 and RNF43 unleashes EGFR-mediated cell growth in 2D culture and**
275 **organoids**
276 EGFR is an important tyrosine kinase that mediates many cellular activities, especially cell growth
277 (Wieduwilt & Moasser, 2008; Yue *et al*, 2021). To study the biological consequence of
278 ZNRF3/RNF43 down-regulating EGFR, we first compared cell growth of WT and
279 *ZNRF3/RNF43*-depleted cells. *Znrf3* knockout in MEFs led to the upregulation of EGFR (Fig. 2B)
280 and an increase in cell growth (Fig. 6A), without affecting canonical WNT signaling activity based
281 on qPCR for WNT target genes (*Sox2*, *Axin2*, *Ccnd1*) (Fig. 6B). EGF and EGFR signaling are also
282 critical for the culture and maintenance of organoids derived from *Apc*-deficient mouse intestinal

283 adenomas (Sato *et al*, 2011), which exhibits constitutively canonical WNT signaling that is no
284 longer modulated by the RSPO-ZNRF3/RNF43 control at the membrane receptor level
285 (Tsukiyama *et al.*, 2021; Tsukiyama *et al*, 2020). Therefore, we established intestinal tumor
286 organoids using the intestinal polyps from the *Apc*^{min} mice (Evans *et al*, 1992) and supplemented
287 RSPO1 in the organoid culture medium to investigate the effect of ZNRF3/RNF43 deactivation
288 on organoid growth and EGFR. Remarkably, the addition of RSPO1 increased the size of *Apc*^{min}
289 mouse intestinal tumor organoids (Fig. 6C and D) in agreement with a previous report (Lahde *et*
290 *al*, 2021) although it did not significantly affect the frequency of organoids detected (Fig. 6E).
291 Immunoblotting analysis confirmed elevated EGFR levels after RSPO1 treatment (Fig. 6F) while
292 qPCR showed no significant increase of *Egfr* nor WNT target genes including *Axin2*, *Myc*, *Sox2*,
293 and *Cd44* (Fig. 6G). Furthermore, we performed functional assays in HT29 cells, which bear *APC*
294 mutations. Overexpression of ZNRF3 in HT29 substantially inhibited cell growth (Fig. 6H) and
295 reduced EGFR levels (Fig. 6I). Conversely, knockout of *RNF43* in HT29 activated multiple EGFR
296 downstream effectors, as RPPA detected increased levels of P-AKT, P-ERK, P-GSK3, P-STAT1,
297 and P-PRAS40 (Fig. S6). Importantly, after confirming abolishment of EGFR phosphorylation
298 (Fig. 6J), the EGFR activity inhibitor erlotinib was found to block the growth gain caused by
299 *RNF43* knockout (Fig. 6K). Together, these data indicate that loss of *ZNRF3* and *RNF43* in cancer
300 cells can promote tumor cell growth through EGFR signaling without significantly engaging
301 canonical WNT signaling.
302
303 **ZNRF3/RNF43 inactivation enhances EGFR and promotes tumor growth *in vivo***
304 To demonstrate the function of the ZNRF3/RNF43-EGFR signaling pathway *in vivo*, we first
305 xenografted luciferase-labeled HT29 cells overexpressing either GFP or ZNRF3 into NSG mice

306 by flank injection and monitored tumor growth by bioluminescence imaging (Fig. 7A). We found
307 that overexpression of ZNRF3 significantly inhibited tumor growth (Fig. 7A). These tumors
308 exhibited decreased EGFR and P-EGFR levels compared to WT tumors (Fig. 7B). However,
309 canonical WNT signaling, based on levels of active-β-Catenin (non-phosphorylated at
310 Ser33/37/Thr41; Fig. 7B), remained unaffected, suggesting that ZNRF3 suppresses tumor growth
311 through down-regulation of EGRF signaling without substantial involvement of canonical WNT
312 signaling.
313
314 Furthermore, we validated this finding in human prostate cancer, where *ZNRF3* and *RNF43* mRNA
315 levels negatively correlated with EGFR protein levels (Fig. 1F). Specifically, we tested whether
316 ZNRF3/RNF43 loss affects EGFR signaling and promotes prostate tumorigenesis *in vivo*. By
317 breeding mice that are floxed at *Znrf3* and *Rnf43* (Koo *et al.*, 2012) with mice transgenic for
318 Probasin-Cre (Wu *et al*, 2001), we generated prostate-specific *Znrf3/Rnf43* knockout mice. At one
319 year of age, these mice exhibited multi-focal prostatic dysplasia and multifocal invasive tumors,
320 as shown by the H&E images (Fig. 7C) and pathological scores (Fig. 7D and S7A-D).
321 Immunohistochemical staining revealed elevated levels of both EGFR and P-EGFR in *Znrf3/Rnf43*
322 knockout prostatic dysplasia and tumors, compared to WT prostate tissues (Fig. 7E), indicating
323 EGFR signaling activation due to *Znrf3/Rnf43* knockout. In contrast, while β-Catenin staining was
324 more intense in knockout tissues and tumors than in WT mice for unknown significance, the β-
325 Catenin signals were mainly restricted to the cell membrane in both WT and *Znrf3/Rnf43* knockout
326 mouse prostate tissues and tumors (Fig. 7E), suggesting no substantial activation of canonical Wnt
327 signaling. Together, these results suggest that loss of *ZNRF/RNF43* elevates EGFR levels and
328 signaling, promoting tumor development.

329

330 **Discussion**

331 The two homologous E3 ubiquitin ligases, ZNRF3 and RNF43, and their antagonistic ligand RSPO
332 have been extensively studied as WNT signaling modulators during normal development and
333 diseases (Basham *et al.*, 2019; Hao *et al.*, 2012; Koo *et al.*, 2012; Lee *et al.*, 2020; Planas-Paz *et*
334 *al.*, 2016; Sun *et al.*, 2021; Szenker-Ravi *et al.*, 2018). Their primary role has been attributed to
335 negatively regulating WNT receptors Frizzled through ubiquitination and degradation (Hao *et al.*,
336 2012; Koo *et al.*, 2012), and the early mass spectrometry analysis of 293T cells following inducible
337 expression of RNF43 only detected downregulation of Frizzled and LRP5 (Koo *et al.*, 2012).
338 However, a few later reports suggested that ZNRF3/RNF43 might also regulate other substrates
339 and exert distinct functions in context-dependent manners. For instance, ZNRF3/RNF43 may
340 induce degradation of BMP receptor BMPR1A (Lee *et al.*, 2020), maternal dorsal determinant
341 Huluwa (Zhu *et al*, 2021), non-canonical WNT component VANGL2 (Radaszkiewicz *et al.*, 2021),
342 and cell adhesion protein E-Cadherin (Zhang *et al*, 2019) in different physiological or pathological
343 conditions. In the context of cancer, *ZNRF3* and *RNF43* are frequently deactivated by gene
344 deletion, mutation, or other means (Hao *et al.*, 2016; Seshagiri *et al.*, 2012). Therefore, this study
345 focused on elucidating ZNRF3/RNF43-regulated signaling pathways in cancer. We discovered
346 that EGFR protein is the most negatively associated with *ZNRF3*/*RNF43* expression using
347 proteogenomic data of cancer patients and that ZNRF3/RNF43 interact with EGFR and down-
348 regulate EGFR through ubiquitination and degradation. Using multiple cell lines and animal
349 models, we demonstrated that loss-of-function changes of ZNRF3/RNF43 elevate EGFR signaling
350 activity to promote cancer progression.

351

352 In colorectal cancer (CRC), *ZNRF3* and *RNF43* mutations occur frequently (Bond *et al.*, 2016;
353 Giannakis *et al.*, 2014; Tu *et al.*, 2019; Vasaikar *et al.*, 2019) and have been mainly associated
354 with the potentiation of WNT signaling (Hao *et al.*, 2016; Hao *et al.*, 2012; Koo *et al.*, 2012).
355 However, our findings suggest that ZNRF3/RNF43 deactivation may unleash other key oncogenic
356 pathways in CRC, especially in the context of APC/CTNNB1 co-mutations that bypass the need
357 for WNT receptor activation for pathway activation (Cerami *et al.*, 2012; Gao *et al.*, 2013). We
358 provide evidence that in human colorectal cancer cells with a hyperactive WNT pathway due to
359 *APC* mutations, knockout of *RNF43* promotes cancer cell growth by activating EGFR signaling.
360 Additionally, we found that the *RNF43* G659Vfs*41 mutant, a hotspot frameshift mutation in
361 human colorectal tumors that may not potentiate WNT signaling (Li *et al*, 2020; Tu *et al.*, 2019),
362 elevates EGFR protein levels, suggesting that this mutation may exert its oncogenic role in cancer
363 through EGFR upregulation. Our data also have clinical implications, as germline polymorphisms
364 and tumor gene expression levels of ZNRF3/RNF43 and RSPO may be related to tumor response
365 to anti-EGFR monoclonal antibody cetuximab-based treatment in CRC patients (Battaglin *et al*,
366 2020), providing insights into understanding the interplay between RSPO-ZNRF3/RNF43 and
367 EGFR protein levels and anti-EGFR activity in CRC treatment.
368
369 By identifying ZNRF3/RNF43 as crucial regulators linking EGFR and WNT signaling at the
370 membrane receptor level, our work reveals a novel mechanism of EGFR and WNT coactivation,
371 which is commonly observed in human cancers (Hu & Li, 2010). Further work should explore the
372 extent to which EGFR and WNT receptors (Frizzled and LRP5/6) each transmit the effect of
373 ZNRF3/RNF43 deactivation at different cancer stages and investigate the efficacy of blocking both
374 EGFR and WNT signaling in treatment of ZNRF3/RNF43-deactivated tumors. Our findings also

375 have implications for organoid culture and normal development. For example, while RSPO and
376 EGF are both required for organoid growth and maintenance, our data suggest that RSPO can both
377 help sustain surface EGFR levels by deactivating ZNRF3/RNF43 and synergize with EGF to boost
378 EGFR signaling activity. Comparative studies on ZNRF3/RNF43 regulation of EGFR versus
379 WNT receptors in terms of substrate abundance, enzyme-substrate binding affinity, *in vivo* ligand
380 availability, and temporal and spatial regulatory mechanisms can provide a comprehensive
381 understanding of the RSPO-ZNRF3/RNF43-regulated signaling network. A recent manuscript
382 reports that RSPO1 addition to *Apc*-deficient mouse intestinal organoids led to an increased size
383 but a decreased number, and implicated abnormal recruitment of the TGF-β/SMAD pathway via
384 LGR5/TGFBRII heterodimers as a mechanism (Lahde *et al*, 2021). We did not detect enhanced
385 TGF-β signaling in our Apc^{min} mouse intestinal tumor culture treated by RSPO1 for two days or
386 eight days (Fig. S8). Furthermore, we did not observe an impact of ZNRF3/RNF43 overexpression
387 on TGFβ receptor I protein levels in our 293T culture studies (Fig. S2B), although our
388 bioinformatic analysis of patient CRCs revealed that SMAD4, a crucial transcription factor
389 downstream of TGF-β receptors, was among the proteins downregulated by ZRNF3/RNF43 (Fig.
390 1C). Therefore, whether TGFβ signaling is directly affected by the RSPO-ZNRF3/RNF43-
391 regulated signaling network needs to be further investigated.
392
393 Structural studies have identified the key amino acids and motifs mediating ZNRF3/RNF43
394 binding with their peptide ligand RSPO (Chen *et al*, 2013; Peng *et al*, 2013; Zebisch *et al*, 2013)
395 and also suggested that RSPO has the closest structural homology with EGFR (domain IV) and
396 insulin receptor (domain II) (Chen *et al.*, 2013). Our co-IP data indicate that ZNRF3/RNF43
397 interact with EGFR through their extracellular domains by co-IP. It would also be interesting to

398 determine further the specific domains and amino acids that are responsible for ZNRF3/RNF43
399 and EGFR interaction and to study whether clinically relevant point mutations at the extracellular
400 domains of ZNRF3/RNF43 and/or EGFR hinder their binding affinity, thereby enhancing EGFR
401 signaling to promote cancer initiation and progression.
402
403 RSPO1-4 bind to both ZNRF3/RNF43 and LGR4/5/6, resulting in ZNRF3/RNF43 auto-
404 ubiquitination and degradation (Hao *et al.*, 2012; Koo *et al.*, 2012). RSPO2/3 can also inhibit
405 ZNRF3/RNF43 independently of LGR4/5/6 (Lebensohn & Rohatgi, 2018; Park *et al.*, 2018;
406 Szenker-Ravi *et al.*, 2018) because RSPO2/3 can bind to the RNF43/ZNRF3 with relatively high
407 affinity, especially in the presence of heparan sulfate proteoglycans (HSPGs) (Dubey *et al.*, 2020).
408 Approximately 18% of CRCs harbor amplification or mutations of *RSPO1-4* or *LGR4/5/6* while
409 10% of CRCs have recurrent *RSPO2/3* gene fusions (Seshagiri *et al.*, 2012). These genetic
410 alterations potentially lead to enhanced inhibition of ZNRF3/RNF43, activating WNT and EGFR
411 signaling (Seeber *et al.*, 2019). While the involvement of each co-receptor (LGR4/5/6; HSPGs) in
412 regulating RSPO-ZNRF3/RNF43 degradation of EGFR requires more investigation, LGR4/5/6
413 may be dispensable for RSPO2-ZNRF3/RNF43 regulation of EGFR because we found that RSPO2
414 mutant that cannot bind to LGR4/5/6 still enhanced EGFR protein levels. It is worth noting that
415 LGR4/5/6 may have a parallel mechanism controlling EGFR levels as we have previously
416 observed that LGR4 can enhance EGFR signaling independently of WNT activation (Yue *et al.*,
417 2021).
418
419 Our work also uncovers a new mechanism of regulating EGFR levels in cancer. Hyperactivation
420 of EGFR in cancer has been attributed to activating mutations, gene amplification, aberrant gene

421 expression, and defective endocytosis/degradation (Nakai *et al*, 2016). But these mechanisms
422 cannot account for all the 60-80% of CRC cases whose EGFR levels are upregulated (Cohen,
423 2003). ZNRF3/RNF43 loss-mediated EGFR stabilization represents a novel mechanism of EGFR
424 upregulation, explaining the elevated EGFR protein levels observed in many human cancers
425 without EGFR gene amplification or overexpression. In our study, ZNRF3/RNF43 can regulate
426 EGFR levels under basal culture conditions as well as with EGF ligand stimulation, but the
427 commonly known EGFR E3 ligase, CBL, mediates ligand-dependent EGFR ubiquitination and
428 degradation (Batzer *et al*, 1994; Duan *et al*, 2011; Grovdal *et al*, 2004; Levkowitz *et al*, 1999;
429 Levkowitz *et al.*, 1998; Waterman *et al*, 2002; Waterman *et al.*, 1999). Therefore, future studies
430 should investigate whether ZNRF3/RNF43 and CBL regulate EGFR ubiquitination and
431 degradation differently, whether ZNRF3/RNF43 regulate both ligand-independent and ligand-
432 dependent EGFR ubiquitination/degradation and consequently affecting different downstream
433 signaling pathways, and whether different EGFR ligands or ligand concentrations direct EGFR to
434 ZNRF3/RNF43 versus CBL for ubiquitination and degradation (Harris *et al*, 2003; Roepstorff *et*
435 *al*, 2009). In addition, a feedback regulation often contributes to tight controls of signaling
436 activation (Chandarlapaty, 2012). In accordance, ZNRF3/RNF43 regulation of WNT signaling is
437 feedback-controlled by *ZNRF3/RNF43* as WNT target genes (Hao *et al.*, 2012; Koo *et al.*, 2012).
438 Whether and how EGFR signaling may affect levels and activities of ZNRF3/RNF43 and their
439 partners including RSPOs and LGRs as a feedback regulation remain to be understood.
440
441 In conclusion, our study unveils a novel ZNRF3/RNF43-EGFR signaling axis in cancer and
442 provides critical insights into RSPO-ZNRF3/RNF43 signaling during cancer progression.
443 Understanding how ZNRF3/RNF43 regulates EGFR and the crosstalk between EGFR and WNT

444 receptors may offer potential therapeutic targets for cancer treatment. Additionally, our findings
445 have implications in organoid culture and normal development, highlighting the significance of
446 RSPO-ZNRF3/RNF43 signaling in various physiological processes. Further research on
447 ZNRF3/RNF43 regulation of EGFR versus WNT receptors in different cancer stages can
448 contribute to a comprehensive understanding of RSPO-ZNRF3/RNF43 signaling in cancer
449 progression and provide valuable knowledge for potential therapeutic interventions.
450

451 **Materials and Methods**

452 **Animal Studies**

453 All experiments using mice were performed utilizing procedures approved by the Institutional
454 Animal Care and Use Committee at Baylor College of Medicine and the Van Andel Institute. The
455 *Rnf43*-flox; *Znrf3*-flox were obtained from the laboratory of Hans Clevers (Koo *et al.*, 2012).
456 CMV-Cre animals were ordered from Jackson Laboratories (JAX stock #006054) (Schwenk *et al*,
457 1995). C57Bl/6J used for backcrossing were ordered from Jackson Laboratories (JAX stock
458 #000664). Probasin-Cre animals were developed in the laboratory of Pradip Roy-Burman (Wu *et*
459 *al.*, 2001). NOD.Cg-Prkdc scid Il2rg tm1Wjl /SzJ (NSG) mice were purchased from Jackson
460 Laboratories (JAX stock #005557) and bred in-house.
461

462 **Cell lines**

463 MDA-MB-231, MDA-MB-468, and HEK293T cells were purchased from ATCC. HT29 and
464 LS180 cells were provided by Q. Liu; HCT116 cells were provided by N. Shroyer; MEF cells were
465 generated from e12.5 embryos using standard methods (Herrera *et al*, 1996). MDA-MB-231,
466 MDA-MB-468, HT29, HCT116, HEK293T, and MEF cells were cultured in DMEM (CORNING,

467 10-013-CV) with 10% FBS and 1% penicillin/streptomycin. LS180 cells were cultured in
468 RPMI1640 (CORNING, 10-013-CV) with 10% FBS and 1% penicillin/streptomycin. All cell lines
469 were routinely tested for mycoplasma contamination.
470
471 **Constructs**
472 Plasmids expressing Flag-FZD5, RNF43, HA-RNF43, or HA-RNF43 (CD8 sp) were provided by
473 Q. Liu. Plasmids expressing Myc-RNF43, Myc-ZNRF3, or Myc-ZNRF3 ΔRING were provided
474 by F. Cong. Plasmids for Myc-ZNRF3-ECD-TM, Myc-ZNRF3-TM-ICD, Myc-ZNRF3 ΔPA, HA-
475 RNF43 ΔPA, HA-RNF43 ΔRING, HA-RNF43-ECD-TM were constructed by subcloning using
476 In-Fusion (TaKaRa, 639642). Plasmids were further constructed for lentiviral expression by
477 subcloning into pBobi vector by In-Fusion.
478
479 **Generation of *RNF43* or *ZNRF3* knockout cancer cell lines**
480 HT29 *RNF43* knockout cells were provided by Q. Liu (guide RNA sequence, g0: 5'-
481 GGCTGCTGATGGCTACCCTGC-3'). Other CRISPR guide sequences for knocking out *RNF43*
482 were designed by http://crispr.mit.edu and cloned into lentiCRISPR v2 (Addgene 52961).
483 Sequences were as follows: g1: 5'-TGGACGCACAGGACTGGTAC-3'; g2: 5'-
484 CAGAGTGATCCCCTTGAAAA-3'; g3: 5'-GGGCAGCCAGCTGCAGCTGG-3'. Lentiviral
485 construct for knocking out *ZNRF3* was provided by Q. Liu (guide RNA sequence, 5'-
486 AGGACTTGTATGAATATGGC-3') (Jiang *et al.*, 2015; Tu *et al.*, 2019). Cancer cells were
487 infected with lentivirus-carrying CRISPR constructs or vector, and then selected in the culture
488 medium containing 2 μg/ml puromycin (InvivoGen, ant-pr-1).
489

490 **Generation of *Znrf3* knockout MEFs**

491 Global null alleles of *Rnf43* and *Znrf3* were generated *in vivo* by crossing *Rnf43*-flox; *Znrf3*-flox
492 mice (Koo *et al.*, 2012) with CMV-Cre (Schwenk *et al.*, 1995). The resulting mice were
493 backcrossed to C57Bl/6J animals to remove the Cre transgene and generate global deletion mouse
494 colonies. Global deletions were confirmed using allele-specific PCR for both *Rnf43* and *Znrf3*.
495 Mouse embryonic fibroblasts (MEFs) were generated using standard protocols (Durkin *et al*, 2013).
496 Briefly, *Rnf43*-KO/+; *Znrf3*-KO/+ mice were crossed, and embryos were collected at E12.5. Yolk
497 sacs were collected for genotyping, and embryo heads and internal organs were removed. The
498 remaining tissue was minced using a razor blade and 0.5mL 0.05% Trypsin-EDTA was added.
499 The suspension was incubated at 37°C for 30 minutes then cultured in MEF media (DMEM, 10%
500 FBS, 1x PenStrep) for subsequent experiments.

501

502 ***Apc*^{min} mouse intestinal tumor organoid culture**

503 Intestinal polyps from 6-month-old female *Apc*^{min} mice (Evans *et al.*, 1992) were isolated and
504 maintained using previously described protocols (Sato *et al.*, 2011; Xue & Shah, 2013), embedded
505 in Matrigel (Corning, 356231), and cultured in basal culture medium (advanced Dulbecco's
506 modified Eagle medium/F12 (Invitrogen, 12634-028), penicillin/streptomycin (Invitrogen, 15140-
507 122), 10 mmol/L HEPES (Invitrogen, 15630-080), 2mM Glutamax (Invitrogen, 35050-061), 1×
508 N2 (Invitrogen, 17502-048), 1× B27 (Invitrogen, 17504-044), 1 mmol/L N-acetylcysteine (Sigma-
509 Aldrich, A9165-5G)) supplemented with 50 ng/ml mouse recombinant EGF (Invitrogen,
510 PMG8043). The organoids were trypsinized with 0.05% Trypsin-EDTA (Invitrogen, 25300054)
511 to obtain single cells, counted and embedded into Matrigel in equal numbers, cultured in basal
512 culture medium supplemented with EGF or basal culture medium supplemented with EGF and 10%

513 RSPO1 conditioned medium for 8 days. The organoids were imaged using Leica DMi8 Inverted
514 Microscope and then harvested for immunoblot analysis.
515
516 **RNA extraction and quantitative PCR**
517 Cells were lysed with TRIzol reagent (Invitrogen, 15596-026). Total RNA was extracted by
518 chloroform and isopropanol precipitation. cDNA was obtained using the SuperScript III First-
519 Strand Synthesis System (Invitrogen, 18080-051). qPCR analyses were performed with primers
520 listed below using SsoAdvanced Universal SYBR Green Supermix (BIO-RAD, 1725270) in at
521 least duplicate in three independent experiments. Plotted are data normalized to *ACTB* or *Actb* and
522 relative to the control. The following primers were used: *ACTB*: 5'-
523 ACTCTTCCAGCCTTCCTTCC-3', 5'-CAGTGATCTCCTTCTGCATCC-3'; *EGFR*: 5'-
524 TGCCCATGAGAAATTTACAGG-3', 5'-ATGTTGCTGAGAAAGTCACTGC-3'; *Actb*: 5'-
525 CATTGCTGACAGGATGCAGAAGG-3', 5'-TGCTGGAAGGTGGACAGTGAGG-3'; *Egfr*: 5′-
526 GGACTGTGTCTCCTGCCAGAAT-3′, 5′-GGCAGACATTCTGGATGGCACT-3′; *Axin2*: 5'-
527 ATGGAGTCCCTCCTTACCGCAT-3', 5'-GTTCCACAGGCGTCATCTCCTT-3'; *Sox2*: 5'-
528 AACGGCAGCTACAGCATGATGC-3', 5'-CGAGCTGGTCATGGAGTTGTAC-3'; *Ccnd1*: 5'-
529 GCAGAAGGAGATTGTGCCATCC-3', 5'-AGGAAGCGGTCCAGGTAGTTCA-3'. The
530 primer sequences for *Tgfbr1*, *Tgfbr2*, *Smad4*, *Ep300*, *Bach1* were from ORIGENE.
531
532 **Flow cytometric analysis**
533 Cells were trypsinized and resuspended in antibody dilution buffer (0.5% BSA in PBS). 5 X 10^5
534 cells were incubated with EGFR (D1D4J) XP Rabbit antibody (PE Conjugate) (Cell Signaling
535 Technology, 48685) for 1 hr at 4 °C. Cells were then washed with antibody dilution buffer and

536 resuspended in antibody dilution buffer. The cells were then subjected to flow cytometry using a
537 BD FACSCanto II (BD, NJ, USA). The resulting data were analyzed using the BD FACSDiva™
538 software.
539
540 **Immunofluorescence**
541 HEK293T cells were seeded on poly-D-lysine coated chamber slides (CORNING, 354632) and
542 transfected with empty vector, or constructs expressing wild-type or fragments of RNF43 or
543 ZNRF3. 48 hr after transfection, cells were fixed in 3.2% paraformaldehyde in PBS at RT for 15
544 min, permeabilized in 3% BSA / 0.1% saponin (Sigma-Aldrich, 47036) in PBS at RT for 30 min,
545 and then incubated in the secondary antibody anti-Rabbit Alex 488 (Invitrogen, A32731) at RT
546 for 1 hr. Afterward, the cells were stained with DAPI (Thermo Fisher Scientific, 62248) and
547 mounted.
548
549 **Immunohistochemistry**
550 Immunochemistry staining was performed using the Vectastain Elite ABC system (Vector
551 Laboratories, Burlingame, CA) and developed using DAB as chromogen (Agilent Dako, Santa
552 Clara, CA, USA). Primary antibodies used in the study included EGFR (D1P9C) rabbit antibody
553 (Mouse Preferred, Cell Signaling Technology, 71655), P-EGFR (Y1068) XP rabbit antibody (Cell
554 Signaling Technology, 2234), Non-phospho (Active) β-Catenin (Ser33/37/Thr41) (D13A1) rabbit
555 antibody (Cell Signaling Technology, 8814).
556
557 **Proximity ligation assay**

558 HCT116 cells were seeded to poly-d-lysine–coated chamber slide (Corning) and co-transfected
559 with Myc-ZNRF3ΔR and EGFR. Two days after transfection, the cells were processed following
560 the standard protocol provided by Sigma-Aldrich (Duolink In Situ Red Starter Kit Mouse/Rabbit).
561 The primary antibodies, EGFR (D38B1) XP rabbit antibody (Cell Signaling Technology, 4267)
562 and Myc-tag (9B11) mouse antibody (Cell Signaling Technology, 2276), were used to detect
563 ZNRF3 and EGFR interaction. For negative control, no primary antibody was used. DAPI was
564 used to stain nuclei. The stained cells were imaged using Leica DMi8 Fluorescence Microscope.
565
566 **Western blot**
567 Cells were lysed on ice using RIPA lysis buffer supplemented with protease inhibitors (Sigma-
568 Aldrich, P8340) and phosphatase inhibitors (Sigma-Aldrich, P5726 and P0044). Cell lysates were
569 then centrifuged at 14,000 rpm for 15 min at 4 °C. Supernatant was collected and the concentration
570 of protein lysate was quantified by BCA assay (Thermo Fisher Scientific, 23225). Cell lysates
571 were mixed with Laemmli sample buffer (BIO-RAD, 1610747) and β-mercaptoethanol (Thermo
572 Fisher Scientific, 21985023) before boiling for 5 min at 95 °C. Equal amounts of protein lysates
573 were loaded and run in 8-12% SDS-PAGE gel. Gels were transferred onto nitrocellulose
574 membrane (Thermo Fisher Scientific, 88018) at 100 V for 90 min at 4 °C. Membranes were then
575 blocked with 5 % non-fat milk in TBST at RT for 1 hr, incubated with primary antibodies overnight
576 at 4 °C and secondary antibodies at RT for 1 hr, and scanned using the Odyssey LI-COR imaging
577 system. Primary antibodies used in the study included EGFR (D38B1) XP rabbit antibody (Cell
578 Signaling Technology, 4267), EGFR (A-10) mouse antibody (Santa Cruz, sc-373746), EGFR
579 (D1P9C) rabbit antibody (Mouse Preferred, Cell Signaling Technology, 71655), P-EGFR (Y1068)
580 XP rabbit antibody (Cell Signaling Technology, 3777), HA-tag mouse antibody (BioLegend

581 901501), HA-tag (C29F4) rabbit antibody (Cell Signaling Technology, 3724), Myc-tag (9B11)
582 mouse antibody (Cell Signaling Technology, 2276), Myc-tag (71D10) rabbit antibody (Cell
583 Signaling Technology, 2278), Flag-tag M2 mouse antibody (Sigma-Aldrich, F1804), Ub (P4D1)
584 mouse antibody (Santa Cruz, sc-8017), CBL mouse antibody (Santa Cruz, sc-1651), Non-phospho
585 (Active) β-Catenin (Ser33/37/Thr41) (D13A1) rabbit antibody (Cell Signaling Technology, 8814),
586 β-Catenin mouse Antibody (BD Biosciences, 610153), GAPDH rabbit antibody (Santa Cruz, sc-
587 25778), β-Actin (Sigma, A5441) and α-Tubulin mouse antibody (Sigma-Aldrich, T9026).
588 Secondary antibodies used included anti-Mouse IRDye 680RD (LI-COR, 926-68070) and anti-
589 Rabbit IRDye 800CW (LI-COR, 926-32211).
590
591 **Immunoprecipitation assay**
592 Cells were lysed on ice using NP-40 or RIPA lysis buffer supplemented with protease inhibitors
593 (Sigma-Aldrich, P8340). Cell lysates were then centrifuged at 14,000 rpm for 15 min at 4 °C.
594 Supernatant was collected and the concentration of protein lysate was quantified by BCA. Protein
595 lysates were incubated with either EGFR (Ab-13) mouse antibody (Thermo Fisher Scientific, MS-
596 609-P1) or Ub (P4D1) mouse antibody (Santa Cruz, sc-8017), and Protein G Sepharose beads (GE
597 Healthcare, 17061801) overnight at 4 °C. Beads were washed with NP-40 or RIPA lysis buffer.
598 Whole-cell lysates and immunoprecipitates were analyzed by western blot analysis.
599
600 **Immunoprecipitation and mass spectrometry**
601 The IP-MS experiments were performed as previously described (Chen *et al*, 2019). BCG823 cells
602 were starved overnight and then treated with 50 ng/ml EGF for 120 mins before sample collection.
603 For each IP experiment, 1 mg protein lysate was incubated with 5 μg EGFR (Ab-13) antibody for

604 2 hr at 4 °C and cleared by ultra-centrifugation (100,000 g, 15min). The supernatant was then
605 incubated with 30 µl 50% protein A-Sepharose slurry (GE Healthcare, 17-0780-01) for 1 hr at 4 °C.
606 The bead-bound complexes were washed 4 times with NETN buffer (20 mM Tris pH7.5, 1 mM
607 EDTA, 0.5% NP-40, 150 mM NaCl) and eluted with 20 µl 2X Laemmli buffer and heated at 95°C
608 for 10 min. IP samples were resolved on a NuPAGE 10% Bis-Tris gel (Life Technologies,
609 WG1201BX10) in 1x MOPS running buffer; the gel was cut into 3 molecular weight regions plus
610 the IgG heavy and light chain bands. Each band was in-gel digested overnight with 100 ng of
611 trypsin which cleaves peptide chains at the C-termini of lysine or arginine in 20 µl of 50 mM
612 NH_4HCO_3 at 37 °C. Peptides were extracted with 350 µl of 100% acetonitrile and 20 µl of 2%
613 formic acid, and dried in a Savant Speed-Vac. Digested peptides were dissolved in 10 µl of loading
614 solution (5% methanol containing 0.1% formic acid) and subjected to LC-MS/MS assay as
615 described previously (Dharmat *et al*, 2018).
616
617 **Reverse phase protein array (RPPA)**
618 RPPA assays were carried out as described previously with minor modifications (Creighton &
619 Huang, 2015). Protein lysates were prepared with modified TPER buffer supplemented with a
620 cocktail of protease and phosphatase inhibitors. Protein lysates at 0.5 mg/ml of total protein were
621 denatured in SDS sample buffer containing 2.5% β-mercaptoethanol at 100 °C for 8 min. The
622 Aushon 2470 Arrayer (Aushon BioSystems) with a 40 pin (185 µm) configuration was used to
623 spot samples and control lysates onto nitrocellulose-coated slides (Grace Bio-labs) using an array
624 format of 960 lysates/slide (2880 spots/slide). The slides were probed with a set of 216 antibodies
625 against total and phospho-proteins using an automated slide stainer Autolink 48 (Dako). Each slide
626 was incubated with one specific primary antibody, and a negative control slide was incubated with

627 antibody diluent instead of primary antibody. Primary antibody binding was detected using a
628 biotinylated secondary antibody followed by streptavidin-conjugated IRDye680 fluorophore (LI-
629 COR Biosciences). Total protein content of each spotted lysate was assessed by fluorescent
630 staining with Sypro Ruby Protein Blot Stain according to the manufacturer's instructions
631 (Molecular Probes). Fluorescence-labeled slides were scanned on a GenePix 4400 AL scanner,
632 along with accompanying negative control slides, at an appropriate PMT to obtain optimal signal
633 for this specific set of samples. The images were analyzed with GenePix Pro 7.0 (Molecular
634 Devices). Total fluorescence signal intensities of each spot were obtained after subtracting the
635 local background signal for each slide and were then normalized for variation in total protein,
636 background and non-specific labeling using a group-based normalization method. For each spot
637 on the array, the background-subtracted foreground signal intensity was subtracted by the
638 corresponding signal intensity of the negative control slide (omission of primary antibody) and
639 then normalized to the corresponding signal intensity of total protein for that spot. Each image and
640 its normalized data were evaluated for quality through manual inspection and control samples.
641 Antibody slides that failed the quality inspection were either repeated at the end of the staining
642 runs or removed before data reporting. Samples (in four biological replicates) were extracted from
643 the normalized data and then log2 transformed. The median value of the three technical replicates
644 was used for statistical analysis. Welch's t-tests were used for group comparisons. FDR-adjusted
645 p-value < 0.05 was considered statistically significant.
646
647 **Subcutaneous xenograft tumor model and IVIS imaging**
648 5 X 10^5 luciferase-labeled HT29 cells were suspended in 0.1 ml serum-free DMEM and injected
649 into the right back flank of 21 to 24-week-old NSG mice. Bioluminescence was measured once a

650 week, by injection of 100 μl 15 mg/ml D-luciferin (LUCNA-1G, Goldbio) via the intra-orbital
651 sinus. Mice were imaged using IVIS Lumina II (Advanced Molecular Vision). The acquired
652 bioluminescence signals were normalized to the day 0 bioluminescence intensity.
653
654 **Statistics**
655 All statistical analyses in our study were conducted using GraphPad Prism or R. Two-tailed t-test
656 without equal variation assumption was used for data comparison between two experimental
657 groups. For data comparison with at least 3 groups, one-way ANOVA test was performed first to
658 assess the overall difference among groups. If differences existed, uncorrected Fisher's LSD test
659 were performed to assess the significance of differences between two groups. Two-way repeated
660 measures ANOVA and uncorrected Fisher's LSD test were used to assess the difference between
661 data sets with time series measurements, including growth curves of cell proliferation and *in vivo*
662 BLI signals. *p*-values less than 0.05 were considered significant.
663
664 **Author contributions**
665 F.Y., X.L., and Y.L. developed the concepts, designed the experiments, interpreted data, and wrote
666 the manuscript. F.Y., A.T.K., P.D.S., M.N.M, W.J., J.T., Z.S., and X.L. performed the experiments.
667 Y.W. performed mass spectrometry analysis. S.H. helped design and performed proteomics
668 experiments. F.Y. and Y. D. performed statistical and bioinformatic analyses. G.H. evaluated
669 slides and provided pathological reports. Q.L., B.O.W., B.Z., N.F.S., X.W, and X-H. F. provided
670 advice, technical expertise, and critical reagents. All authors read and approved the final
671 manuscript.
672

673 **Competing interests** Authors declare that they have no competing interests.

674

675 **Data and materials availability** All data are available in the main text or the supplementary

676 materials.

677

678 **Acknowledgments** We thank Dr. Feng Cong for the generous gifts of reagents. We also thank Dr.

679 Xuan Wang from the BCM Antibody-based Proteomics Core/Shared Resource for her technical

680 assistance in performing reverse phase protein array; Ms. Xi-Lei Zeng and Ms. Xiaomin Yu from

681 the Texas Medical Digestive Diseases Center (DDC) GEMS core for assistance in organoid culture;

682 Ms. Cassandra Diegel from the Van Andel Institute for assistance. This work was financially

683 supported by NIH/NCI (R01 CA204926 and CA271498 to Y.L.), DOD-CDMRP (BC191649 and

684 BC191646 to Y.L.), and NIH-T32 grant (#1T32CA203690-01A1 to A.K. under Dr. Suzanne

685 Fuqua). This project was also supported by the Breast Center Pathology Core as part of the SPORE

686 program (P50 CA186784), Cytometry and Cell Sorting Core with funding from CPRIT (RP180672)

687 and NIH (S10 RR024574), Antibody-based Proteomics Core with funding from CPRIT

688 (RP210227) and NIH (S10 OD028648 to S.H.), DDC GEMS core with funding from NIH/NIDDK

689 (DK56338), and resources from the Dan L. Duncan Cancer Center with funding from NIH/NCI

690 (P30 CA125123). The Van Andel Institute (VAI) provided additional support, including

691 contributions from the VAI Vivarium (RRID:SCR_023211) and VAI Pathology and Biorepository

692 Core (RRID:SCR_022912). P.D.S was supported by a post-doctoral fellowship from the American

693 Cancer Society (PF-20-109-01) and M.N.M is supported by the NIH/NIDCR (K08DE3109).

694

695 **Reference**

696 Assie G, Letouze E, Fassnacht M, Jouinot A, Luscap W, Barreau O, Omeiri H, Rodriguez S,
697 Perlemoine K, Rene-Corail F *et al* (2014) Integrated genomic characterization of adrenocortical
698 carcinoma. *Nat Genet* 46: 607-612
699 Basham KJ, Rodriguez S, Turcu AF, Lerario AM, Logan CY, Rysztak MR, Gomez-Sanchez CE,
700 Breault DT, Koo BK, Clevers H *et al* (2019) A ZNRF3-dependent Wnt/beta-catenin signaling
701 gradient is required for adrenal homeostasis. *Genes & development* 33: 209-220
702 Battaglin F, Xiao Y, Millstein J, Seeber A, Arai H, Wang J, Puccini A, Tokunaga R, Naseem M, Soni
703 S *et al* (2020) Genetic variants in R-Spondin/RNF43 complex and gene expression levels to
704 predict efficacy of cetuximab (cet) in patients (pts) with metastatic colorectal cancer (mCRC):
705 Data from the FIRE-3 phase III trial. *Journal of Clinical Oncology* 38: 190-190
706 Batzer AG, Rotin D, Urena JM, Skolnik EY, Schlessinger J (1994) Hierarchy of binding sites for
707 Grb2 and Shc on the epidermal growth factor receptor. *Mol Cell Biol* 14: 5192-5201
708 Bond CE, McKeone DM, Kalimutho M, Bettington ML, Pearson SA, Dumenil TD, Wockner LF,
709 Burge M, Leggett BA, Whitehall VL (2016) RNF43 and ZNRF3 are commonly altered in serrated
710 pathway colorectal tumorigenesis. *Oncotarget* 7: 70589-70600
711 Carmon KS, Gong X, Lin Q, Thomas A, Liu Q (2011) R-spondins function as ligands of the orphan
712 receptors LGR4 and LGR5 to regulate Wnt/beta-catenin signaling. *Proceedings of the National*
713 *Academy of Sciences of the United States of America* 108: 11452-11457
714 Cerami E, Gao J, Dogrusoz U, Gross BE, Sumer SO, Aksoy BA, Jacobsen A, Byrne CJ, Heuer ML,
715 Larsson E *et al* (2012) The cBio cancer genomics portal: an open platform for exploring
716 multidimensional cancer genomics data. *Cancer Discov* 2: 401-404
717 Chandarlapaty S (2012) Negative feedback and adaptive resistance to the targeted therapy of
718 cancer. *Cancer Discov* 2: 311-319
719 Chen PH, Chen X, Lin Z, Fang D, He X (2013) The structural basis of R-spondin recognition by
720 LGR5 and RNF43. *Genes & development* 27: 1345-1350
721 Chen Y, Leng M, Gao Y, Zhan D, Choi JM, Song L, Li K, Xia X, Zhang C, Liu M *et al* (2019) A Cross-
722 Linking-Aided Immunoprecipitation/Mass Spectrometry Workflow Reveals Extensive
723 Intracellular Trafficking in Time-Resolved, Signal-Dependent Epidermal Growth Factor Receptor
724 Proteome. *J Proteome Res* 18: 3715-3730
725 Cohen RB (2003) Epidermal growth factor receptor as a therapeutic target in colorectal cancer.
726 *Clin Colorectal Cancer* 2: 246-251
727 Creighton CJ, Huang S (2015) Reverse phase protein arrays in signaling pathways: a data
728 integration perspective. *Drug design, development and therapy* 9: 3519-3527
729 de Lau W, Barker N, Low TY, Koo BK, Li VS, Teunissen H, Kujala P, Haegebarth A, Peters PJ, van
730 de Wetering M *et al* (2011) Lgr5 homologues associate with Wnt receptors and mediate R-
731 spondin signalling. *Nature* 476: 293-297
732 Dharmat R, Eblimit A, Robichaux MA, Zhang Z, Nguyen TT, Jung SY, He F, Jain A, Li Y, Qin J *et al*
733 (2018) SPATA7 maintains a novel photoreceptor-specific zone in the distal connecting cilium. *J*
734 *Cell Biol* 217: 2851-2865
735 Duan L, Raja SM, Chen G, Virmani S, Williams SH, Clubb RJ, Mukhopadhyay C, Rainey MA, Ying
736 G, Dimri M *et al* (2011) Negative regulation of EGFR-Vav2 signaling axis by Cbl ubiquitin ligase

controls EGF receptor-mediated epithelial cell adherens junction dynamics and cell migration. *J Biol Chem* 286: 620-633

Dubey R, van Kerkhof P, Jordens I, Malinauskas T, Pusapati GV, McKenna JK, Li D, Carette JE, Ho M, Siebold C *et al* (2020) R-spondins engage heparan sulfate proteoglycans to potentiate WNT signaling. *Elife* 9

Durkin ME, Qian X, Popescu NC, Lowy DR (2013) Isolation of Mouse Embryo Fibroblasts. *Bio Protoc* 3

Eto T, Miyake K, Nosho K, Ohmuraya M, Imamura Y, Arima K, Kanno S, Fu L, Kiyozumi Y, Izumi D *et al* (2018) Impact of loss-of-function mutations at the RNF43 locus on colorectal cancer development and progression. *J Pathol* 245: 445-455

Evans GS, Flint N, Somers AS, Eyden B, Potten CS (1992) The development of a method for the preparation of rat intestinal epithelial cell primary cultures. *J Cell Sci* 101 (Pt 1): 219-231

Fang L, Ford-Roshon D, Russo M, O'Brien C, Xiong X, Gurjao C, Grandclaudon M, Raghavan S, Corsello SM, Carr SA *et al* (2022) RNF43 G659fs is an oncogenic colorectal cancer mutation and sensitizes tumor cells to PI3K/mTOR inhibition. *Nat Commun* 13: 3181

Galcheva-Gargova Z, Theroux SJ, Davis RJ (1995) The epidermal growth factor receptor is covalently linked to ubiquitin. *Oncogene* 11: 2649-2655

Gao J, Aksoy BA, Dogrusoz U, Dresdner G, Gross B, Sumer SO, Sun Y, Jacobsen A, Sinha R, Larsson E *et al* (2013) Integrative analysis of complex cancer genomics and clinical profiles using the cBioPortal. *Sci Signal* 6: pl1

Geng A, Wu T, Cai C, Song W, Wang J, Yu QC, Zeng YA (2020) A novel function of R-spondin1 in regulating estrogen receptor expression independent of Wnt/beta-catenin signaling. *Elife* 9

Giannakis M, Hodis E, Jasmine Mu X, Yamauchi M, Rosenbluh J, Cibulskis K, Saksena G, Lawrence MS, Qian ZR, Nishihara R *et al* (2014) RNF43 is frequently mutated in colorectal and endometrial cancers. *Nat Genet* 46: 1264-1266

Glinka A, Dolde C, Kirsch N, Huang YL, Kazanskaya O, Ingelfinger D, Boutros M, Cruciat CM, Niehrs C (2011) LGR4 and LGR5 are R-spondin receptors mediating Wnt/beta-catenin and Wnt/PCP signalling. *EMBO Rep* 12: 1055-1061

Grovdal LM, Stang E, Sorkin A, Madshus IH (2004) Direct interaction of Cbl with pTyr 1045 of the EGF receptor (EGFR) is required to sort the EGFR to lysosomes for degradation. *Exp Cell Res* 300: 388-395

Hao HX, Jiang X, Cong F (2016) Control of Wnt Receptor Turnover by R-spondin-ZNRF3/RNF43 Signaling Module and Its Dysregulation in Cancer. *Cancers (Basel)* 8

Hao HX, Xie Y, Zhang Y, Charlat O, Oster E, Avello M, Lei H, Mickanin C, Liu D, Ruffner H *et al* (2012) ZNRF3 promotes Wnt receptor turnover in an R-spondin-sensitive manner. *Nature* 485: 195-200

Harris A, Siggers P, Corrochano S, Warr N, Sagar D, Grimes DT, Suzuki M, Burdine RD, Cong F, Koo BK *et al* (2018) ZNRF3 functions in mammalian sex determination by inhibiting canonical WNT signaling. *Proceedings of the National Academy of Sciences of the United States of America* 115: 5474-5479

Harris RC, Chung E, Coffey RJ (2003) EGF receptor ligands. *Exp Cell Res* 284: 2-13

Herrera RE, Sah VP, Williams BO, Mäkelä TP, Weinberg RA, Jacks T (1996) Altered cell cycle kinetics, gene expression, and G1 restriction point regulation in Rb-deficient fibroblasts. *Mol Cell Biol* 16: 2402-2407

781 Hu T, Li C (2010) Convergence between Wnt-beta-catenin and EGFR signaling in cancer. *Mol*
782 *Cancer* 9: 236
783 Jiang X, Charlat O, Zamponi R, Yang Y, Cong F (2015) Dishevelled promotes Wnt receptor
784 degradation through recruitment of ZNRF3/RNF43 E3 ubiquitin ligases. *Mol Cell* 58: 522-533
785 Jiang X, Hao HX, Growney JD, Woolfenden S, Bottiglio C, Ng N, Lu B, Hsieh MH, Bagdasarian L,
786 Meyer R *et al* (2013) Inactivating mutations of RNF43 confer Wnt dependency in pancreatic
787 ductal adenocarcinoma. *Proceedings of the National Academy of Sciences of the United States*
788 *of America* 110: 12649-12654
789 Klauzinska M, Baljinnyam B, Raafat A, Rodriguez-Canales J, Strizzi L, Greer YE, Rubin JS, Callahan
790 R (2012) Rspo2/Int7 regulates invasiveness and tumorigenic properties of mammary epithelial
791 cells. *J Cell Physiol* 227: 1960-1971
792 Koo BK, Spit M, Jordens I, Low TY, Stange DE, van de Wetering M, van Es JH, Mohammed S,
793 Heck AJ, Maurice MM *et al* (2012) Tumour suppressor RNF43 is a stem-cell E3 ligase that
794 induces endocytosis of Wnt receptors. *Nature* 488: 665-669
795 Lahde M, Heino S, Hogstrom J, Kaijalainen S, Anisimov A, Flanagan D, Kallio P, Leppanen VM,
796 Ristimaki A, Ritvos O *et al* (2021) Expression of R-Spondin 1 in Apc(Min/+) Mice Suppresses
797 Growth of Intestinal Adenomas by Altering Wnt and Transforming Growth Factor Beta
798 Signaling. *Gastroenterology* 160: 245-259
799 Lebensohn AM, Rohatgi R (2018) R-spondins can potentiate WNT signaling without LGRs. *Elife* 7
800 Lee H, Seidl C, Sun R, Glinka A, Niehrs C (2020) R-spondins are BMP receptor antagonists in
801 Xenopus early embryonic development. *Nat Commun* 11: 5570
802 Levkowitz G, Waterman H, Ettenberg SA, Katz M, Tsygankov AY, Alroy I, Lavi S, Iwai K, Reiss Y,
803 Ciechanover A *et al* (1999) Ubiquitin ligase activity and tyrosine phosphorylation underlie
804 suppression of growth factor signaling by c-Cbl/Sli-1. *Mol Cell* 4: 1029-1040
805 Levkowitz G, Waterman H, Zamir E, Kam Z, Oved S, Langdon WY, Beguinot L, Geiger B, Yarden Y
806 (1998) c-Cbl/Sli-1 regulates endocytic sorting and ubiquitination of the epidermal growth factor
807 receptor. *Genes & development* 12: 3663-3674
808 Li S, Lavrijsen M, Bakker A, Magierowski M, Magierowska K, Liu P, Wang W, Peppelenbosch MP,
809 Smits R (2020) Commonly observed RNF43 mutations retain functionality in attenuating
810 Wnt/beta-catenin signaling and unlikely confer Wnt-dependency onto colorectal cancers.
811 *Oncogene* 39: 3458-3472
812 Lienert F, Mohn F, Tiwari VK, Baubec T, Roloff TC, Gaidatzis D, Stadler MB, Schubeler D (2011)
813 Genomic prevalence of heterochromatic H3K9me2 and transcription do not discriminate
814 pluripotent from terminally differentiated cells. *PLoS Genet* 7: e1002090
815 Mastrogiovanni G, Pacini C, Kakava S, Arnes-Benito R, Bradshaw CR, Davies S, Saeb-Parsy K, Koo
816 B-K, Huch M (2020) Loss of RNF43/ZNRF3 predisposes to Hepatocellular carcinoma by impairing
817 liver regeneration and altering liver fat metabolism. *bioRxiv*: 2020.2009.2025.313205
818 Mulvaney JF, Yatteau A, Sun WW, Jacques B, Takubo K, Suda T, Yamada W, Dabdoub A (2013)
819 Secreted factor R-Spondin 2 is involved in refinement of patterning of the mammalian cochlea.
820 *Dev Dyn* 242: 179-188
821 Nakai K, Hung MC, Yamaguchi H (2016) A perspective on anti-EGFR therapies targeting triple-
822 negative breast cancer. *Am J Cancer Res* 6: 1609-1623

823 Neumeyer V, Brutau-Abia A, Allgauer M, Pfarr N, Weichert W, Falkeis-Veits C, Kremmer E, Vieth
824 M, Gerhard M, Mejias-Luque R (2020) Loss of RNF43 Function Contributes to Gastric
825 Carcinogenesis by Impairing DNA Damage Response. *Cell Mol Gastroenterol Hepatol*
826 Neumeyer V, Grandl M, Dietl A, Brutau-Abia A, Allgauer M, Kalali B, Zhang Y, Pan KF, Steiger K,
827 Vieth M *et al* (2019) Loss of endogenous RNF43 function enhances proliferation and tumour
828 growth of intestinal and gastric cells. *Carcinogenesis* 40: 551-559
829 Pangestu NS, Chueakwon P, Talabnin K, Khiaowichit J, Talabnin C (2021) RNF43 overexpression
830 attenuates the Wnt/beta-catenin signalling pathway to suppress tumour progression in
831 cholangiocarcinoma. *Oncol Lett* 22: 846
832 Park S, Cui J, Yu W, Wu L, Carmon KS, Liu QJ (2018) Differential activities and mechanisms of the
833 four R-spondins in potentiating Wnt/beta-catenin signaling. *J Biol Chem* 293: 9759-9769
834 Park S, Wu L, Tu J, Yu W, Toh Y, Carmon KS, Liu QJ (2020) Unlike LGR4, LGR5 potentiates Wnt-
835 beta-catenin signaling without sequestering E3 ligases. *Sci Signal* 13
836 Peng WC, de Lau W, Madoori PK, Forneris F, Granneman JC, Clevers H, Gros P (2013) Structures
837 of Wnt-antagonist ZNRF3 and its complex with R-spondin 1 and implications for signaling. *PLoS*
838 *One* 8: e83110
839 Pickart CM, Eddins MJ (2004) Ubiquitin: structures, functions, mechanisms. *Biochim Biophys*
840 *Acta* 1695: 55-72
841 Planas-Paz L, Orsini V, Boulter L, Calabrese D, Pikiolek M, Nigsch F, Xie Y, Roma G, Donovan A,
842 Marti P *et al* (2016) The RSPO-LGR4/5-ZNRF3/RNF43 module controls liver zonation and size.
843 *Nat Cell Biol* 18: 467-479
844 Qiu W, Yang Z, Fan Y, Zheng Q (2016) ZNRF3 is downregulated in papillary thyroid carcinoma
845 and suppresses the proliferation and invasion of papillary thyroid cancer cells. *Tumour Biol* 37:
846 12665-12672
847 Radaszkiewicz T, Bryja V (2020) Protease associated domain of RNF43 is not necessary for the
848 suppression of Wnt/beta-catenin signaling in human cells. *Cell Commun Signal* 18: 91
849 Radaszkiewicz T, Noskova M, Gomoryova K, Vondalova Blanarova O, Radaszkiewicz KA, Pickova
850 M, Vichova R, Gybel T, Kaiser K, Demkova L *et al* (2021) RNF43 inhibits WNT5A-driven signaling
851 and suppresses melanoma invasion and resistance to the targeted therapy. *Elife* 10
852 Roepstorff K, Grandal MV, Henriksen L, Knudsen SL, Lerdrup M, Grovdal L, Willumsen BM, van
853 Deurs B (2009) Differential effects of EGFR ligands on endocytic sorting of the receptor. *Traffic*
854 10: 1115-1127
855 Sato T, Stange DE, Ferrante M, Vries RG, Van Es JH, Van den Brink S, Van Houdt WJ, Pronk A,
856 Van Gorp J, Siersema PD *et al* (2011) Long-term expansion of epithelial organoids from human
857 colon, adenoma, adenocarcinoma, and Barrett's epithelium. *Gastroenterology* 141: 1762-1772
858 Schwenk F, Baron U, Rajewsky K (1995) A cre-transgenic mouse strain for the ubiquitous
859 deletion of loxP-flanked gene segments including deletion in germ cells. *Nucleic Acids Res* 23:
860 5080-5081
861 Seeber A, Kocher F, Xiu J, Spizzo G, Puccini A, Swensen J, Ellis M, Goldberg RM, Grothey A,
862 Shields AF *et al* (2019) Molecular landscape of colorectal cancers harboring R-spondin fusions.
863 *Journal of Clinical Oncology* 37: 3588-3588
864 Seshagiri S, Stawiski EW, Durinck S, Modrusan Z, Storm EE, Conboy CB, Chaudhuri S, Guan Y,
865 Janakiraman V, Jaiswal BS *et al* (2012) Recurrent R-spondin fusions in colon cancer. *Nature* 488:
866 660-664

867 Sun T, Annunziato S, Bergling S, Sheng C, Orsini V, Forcella P, Pikiolek M, Kancherla V, Holwerda
868 S, Imanci D *et al* (2021) ZNRF3 and RNF43 cooperate to safeguard metabolic liver zonation and
869 hepatocyte proliferation. *Cell Stem Cell* 28: 1822-1837 e1810
870 Szenker-Ravi E, Altunoglu U, Leushacke M, Bosso-Lefevre C, Khatoo M, Thi Tran H, Naert T,
871 Noelanders R, Hajamohideen A, Beneteau C *et al* (2018) RSPO2 inhibition of RNF43 and ZNRF3
872 governs limb development independently of LGR4/5/6. *Nature* 557: 564-569
873 Tsukiyama T, Fukui A, Terai S, Fujioka Y, Shinada K, Takahashi H, Yamaguchi TP, Ohba Y,
874 Hatakeyama S (2015) Molecular Role of RNF43 in Canonical and Noncanonical Wnt Signaling.
875 *Mol Cell Biol* 35: 2007-2023
876 Tsukiyama T, Koo BK, Hatakeyama S (2021) Post-translational Wnt receptor regulation: Is the
877 fog slowly clearing?: The molecular mechanism of RNF43/ZNRF3 ubiquitin ligases is not yet fully
878 elucidated and still controversial. *Bioessays* 43: e2000297
879 Tsukiyama T, Zou J, Kim J, Ogamino S, Shino Y, Masuda T, Merenda A, Matsumoto M, Fujioka Y,
880 Hirose T *et al* (2020) A phospho-switch controls RNF43-mediated degradation of Wnt receptors
881 to suppress tumorigenesis. *Nat Commun* 11: 4586
882 Tu J, Park S, Yu W, Zhang S, Wu L, Carmon K, Liu QJ (2019) The most common RNF43 mutant
883 G659Vfs*41 is fully functional in inhibiting Wnt signaling and unlikely to play a role in
884 tumorigenesis. *Sci Rep* 9: 18557
885 Vasaikar S, Huang C, Wang X, Petyuk VA, Savage SR, Wen B, Dou Y, Zhang Y, Shi Z, Arshad OA *et*
886 *al* (2019) Proteogenomic Analysis of Human Colon Cancer Reveals New Therapeutic
887 Opportunities. *Cell* 177: 1035-1049 e1019
888 Vasaikar SV, Straub P, Wang J, Zhang B (2018) LinkedOmics: analyzing multi-omics data within
889 and across 32 cancer types. *Nucleic Acids Res* 46: D956-D963
890 Waterman H, Katz M, Rubin C, Shtiegman K, Lavi S, Elson A, Jovin T, Yarden Y (2002) A mutant
891 EGF-receptor defective in ubiquitylation and endocytosis unveils a role for Grb2 in negative
892 signaling. *EMBO J* 21: 303-313
893 Waterman H, Levkowitz G, Alroy I, Yarden Y (1999) The RING finger of c-Cbl mediates
894 desensitization of the epidermal growth factor receptor. *J Biol Chem* 274: 22151-22154
895 Wieduwilt MJ, Moasser MM (2008) The epidermal growth factor receptor family: biology
896 driving targeted therapeutics. *Cell Mol Life Sci* 65: 1566-1584
897 Wu X, Wu J, Huang J, Powell WC, Zhang J, Matusik RJ, Sangiorgi FO, Maxson RE, Sucov HM, Roy-
898 Burman P (2001) Generation of a prostate epithelial cell-specific Cre transgenic mouse model
899 for tissue-specific gene ablation. *Mech Dev* 101: 61-69
900 Xie Y, Zamponi R, Charlat O, Ramones M, Swalley S, Jiang X, Rivera D, Tschantz W, Lu B, Quinn L
901 *et al* (2013) Interaction with both ZNRF3 and LGR4 is required for the signalling activity of R-
902 spondin. *EMBO Rep* 14: 1120-1126
903 Xue X, Shah YM (2013) In vitro organoid culture of primary mouse colon tumors. *J Vis Exp*:
904 e50210
905 Yan KS, Janda CY, Chang J, Zheng GXY, Larkin KA, Luca VC, Chia LA, Mah AT, Han A, Terry JM *et*
906 *al* (2017) Non-equivalence of Wnt and R-spondin ligands during Lgr5(+) intestinal stem-cell self-
907 renewal. *Nature* 545: 238-242
908 Yu J, Yusoff PAM, Woutersen DTJ, Goh P, Harmston N, Smits R, Epstein DM, Virshup DM, Madan
909 B (2020) The Functional Landscape of Patient-Derived RNF43 Mutations Predicts Sensitivity to
910 Wnt Inhibition. *Cancer Res* 80: 5619-5632

911 Yue F, Jiang W, Ku AT, Young AIJ, Zhang W, Souto EP, Gao Y, Yu Z, Wang Y, Creighton CJ *et al*
912 (2021) A Wnt-Independent LGR4-EGFR Signaling Axis in Cancer Metastasis. *Cancer Res* 81:
913 4441-4454
914 Zebisch M, Xu Y, Krastev C, MacDonald BT, Chen M, Gilbert RJ, He X, Jones EY (2013) Structural
915 and molecular basis of ZNRF3/RNF43 transmembrane ubiquitin ligase inhibition by the Wnt
916 agonist R-spondin. *Nat Commun* 4: 2787
917 Zhang Y, Sun L, Gao X, Guo A, Diao Y, Zhao Y (2019) RNF43 ubiquitinates and degrades
918 phosphorylated E-cadherin by c-Src to facilitate epithelial-mesenchymal transition in lung
919 adenocarcinoma. *BMC Cancer* 19: 670
920 Zhou Y, Lan J, Wang W, Shi Q, Lan Y, Cheng Z, Guan H (2013) ZNRF3 acts as a tumour suppressor
921 by the Wnt signalling pathway in human gastric adenocarcinoma. *J Mol Histol* 44: 555-563
922 Zhu X, Wang P, Wei J, Li Y, Zhai J, Zheng T, Tao Q (2021) Lysosomal degradation of the maternal
923 dorsal determinant Hwa safeguards dorsal body axis formation. *EMBO Rep* 22: e53185
924

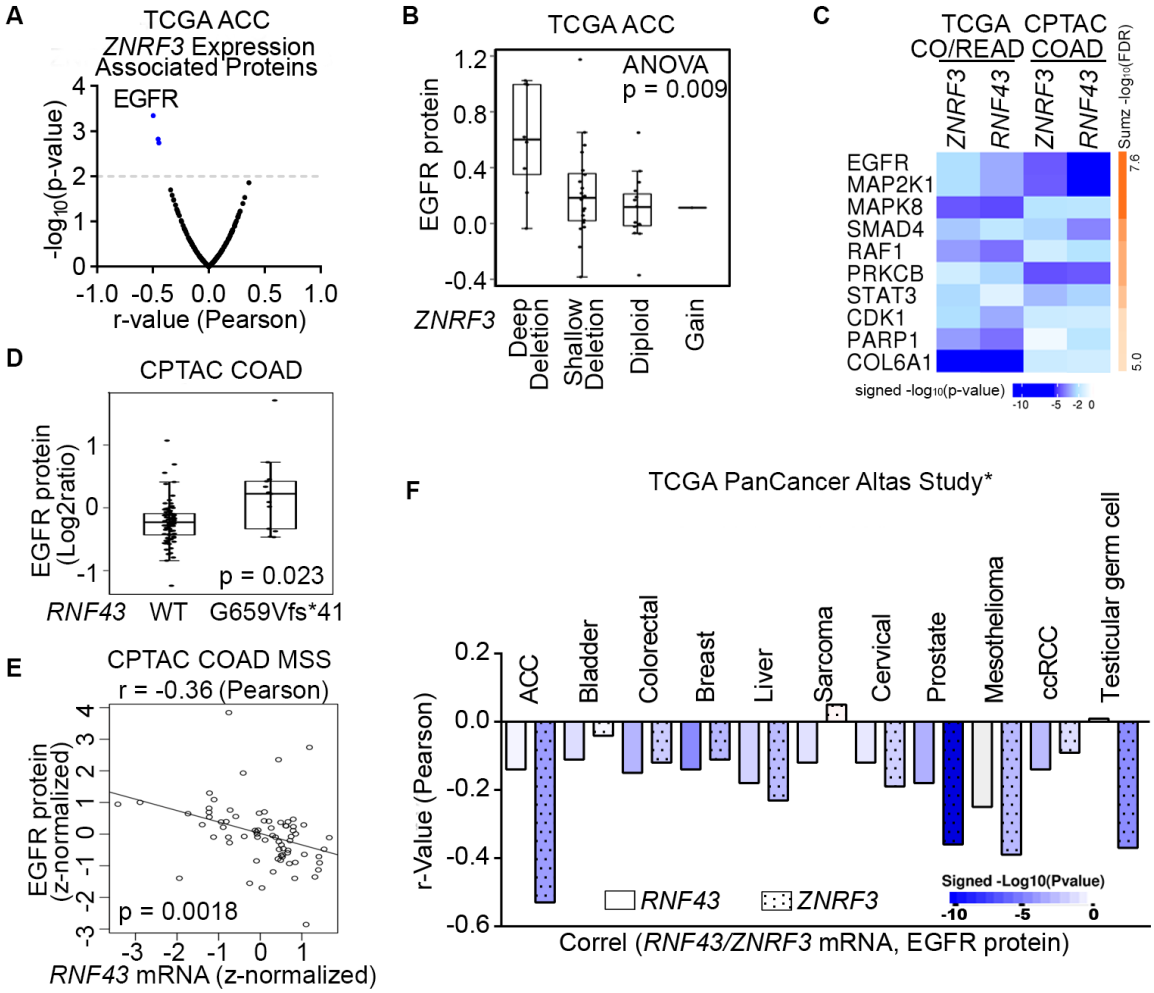
A
TCGA ACC
ZNRF3 Expression
Associated Proteins
EGFR
-log10(p-value)
r-value (Pearson)
B
TCGA ACC
ANOVA
p = 0.009
EGFR protein
ZNRF3
Deep Deletion
Shallow Deletion
Diploid
Gain
C
TCGA CO/READ
CPTAC COAD
ZNRF3
RNF43
ZNRF3
RNF43
Sumz -log10(FDR)
EGFR
MAP2K1
MAPK8
SMAD4
RAF1
PRKCB
STAT3
CDK1
PARP1
COL6A1
signed -log10(p-value)
D
CPTAC COAD
EGFR protein (Log2ratio)
p = 0.023
RNF43
WT
G659Vfs*41
E
CPTAC COAD MSS
r = -0.36 (Pearson)
EGFR protein (z-normalized)
p = 0.0018
RNF43 mRNA (z-normalized)
F
TCGA PanCancer Altas Study*
ACC
Bladder
Colorectal
Breast
Liver
Sarcoma
Cervical
Prostate
Mesothelioma
ccRCC
Testicular germ cell
r-Value (Pearson)
RNF43
ZNRF3
Signed -Log10(Pvalue)
Correl (RNF43/ZNRF3 mRNA, EGFR protein)

925

926

927 Fig.1 Proteogenomic analysis identifies EGFR as the top candidate protein down-regulated by
928 ZNRF3/RNF43 in cancers.
929 **A**, Volcano plot of proteins associated with *ZNRF3* mRNA expression in human adrenal cortical
930 carcinoma (ACC), using the TCGA dataset (n = 92).
931 **B**, Boxplot of EGFR protein levels in human adrenal cortical carcinomas with different *ZNRF3*
932 gene copy number alteration, using the TCGA dataset (n = 92).
933 **C**, The top ten proteins negatively correlated with *ZNRF3/RNF43* mRNA levels, ranked by
934 Stouffer's method, using the TCGA colorectal adenocarcinoma (CO/READ) (n = 629) and the
935 CPTAC colon adenocarcinoma (COAD) (n = 210) datasets.
936 **D**. Boxplot of EGFR protein levels in human colon adenocarcinomas expressing RNF43 WT or
937 G659Vfs*41 mutant, using the CPTAC dataset.
938 **E**. Scatterplot of EGFR protein level versus *RNF43* mRNA expression using microsatellite stable
939 (MSS) colon adenocarcinoma in the CPTAC dataset.
940 **F**. Bar graph of significant associations between *RNF43*/*ZNRF3* mRNA expression and EGFR
941 protein level in cancer datasets from TCGA PanCancer Altas Study. *, insignificant associations
942 were not shown.
943

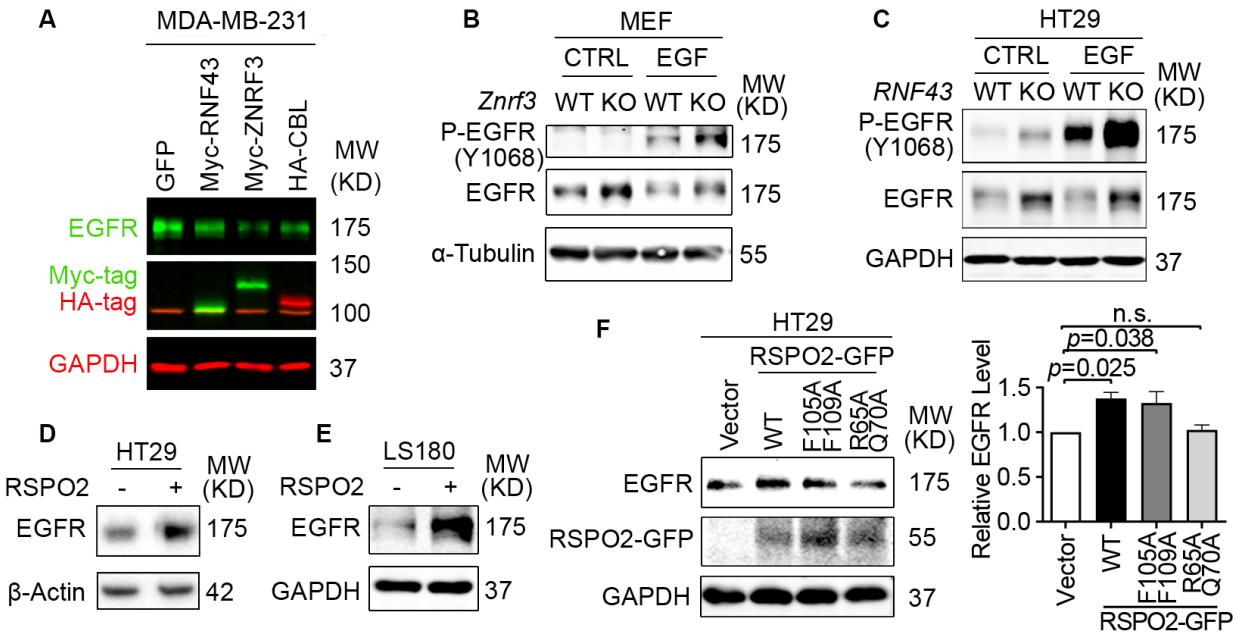
A
MDA-MB-231
GFP
Myc-RNF43
Myc-ZNRF3
HA-CBL
MW (KD)
EGFR
175
Myc-tag
150
HA-tag
100
GAPDH
37
B
MEF
CTRL
EGF
Znrf3
WT KO WT KO
MW (KD)
P-EGFR (Y1068)
175
EGFR
175
α-Tubulin
55
C
HT29
CTRL
EGF
RNF43
WT KO WT KO
MW (KD)
P-EGFR (Y1068)
175
EGFR
175
GAPDH
37
D
HT29
RSPO2
- +
MW (KD)
EGFR
175
β-Actin
42
E
LS180
RSPO2
- +
MW (KD)
EGFR
175
GAPDH
37
F
HT29
RSPO2-GFP
Vector
WT
F105A F109A
R65A Q70A
MW (KD)
EGFR
175
RSPO2-GFP
55
GAPDH
37
n.s.
p=0.038
p=0.025
Relative EGFR Level
1.5
1.0
0.5
0.0
Vector
WT
F105A F109A
R65A Q70A
RSPO2-GFP

947 Fig.2 ZNRF3/RNF43 downregulates EGFR protein level.

948 **A**. Overexpression of RNF43, ZNRF3, or CBL decreases EGFR protein level compared to GFP
949 control in MDA-MB-231 cells. Cells were infected with lentivirus expressing GFP, or E3 ligases.

950 **B**. *Znrf3* knockout increases P-EGFR and total EGFR levels in MEFs upon EGF stimulation (50
951 ng/ml, 10 min).

952 **C**. *RNF43* knockout increases P-EGFR and total EGFR levels in HT29 cells untreated or treated
953 with recombinant EGF (50 ng/ml, 10 min).

954 **D, E**. RSPO2 treatment (50 ng/ml, 2-4 hr) enhances EGFR protein levels in HT29 (**D**) and LS180
955 (**E**) cells.

956 **F**. Overexpression of RSPO2 WT or F105A/F109A mutant but R65A/Q70A mutant enhances
957 EGFR protein level, shown by representative western blot images (left panel) and quantification
958 results (right panel).

959 Means ± SEMs are shown. *p*-values were calculated by one-way ANOVA uncorrected Fisher's
960 LSD test. n.s., not significant.

961

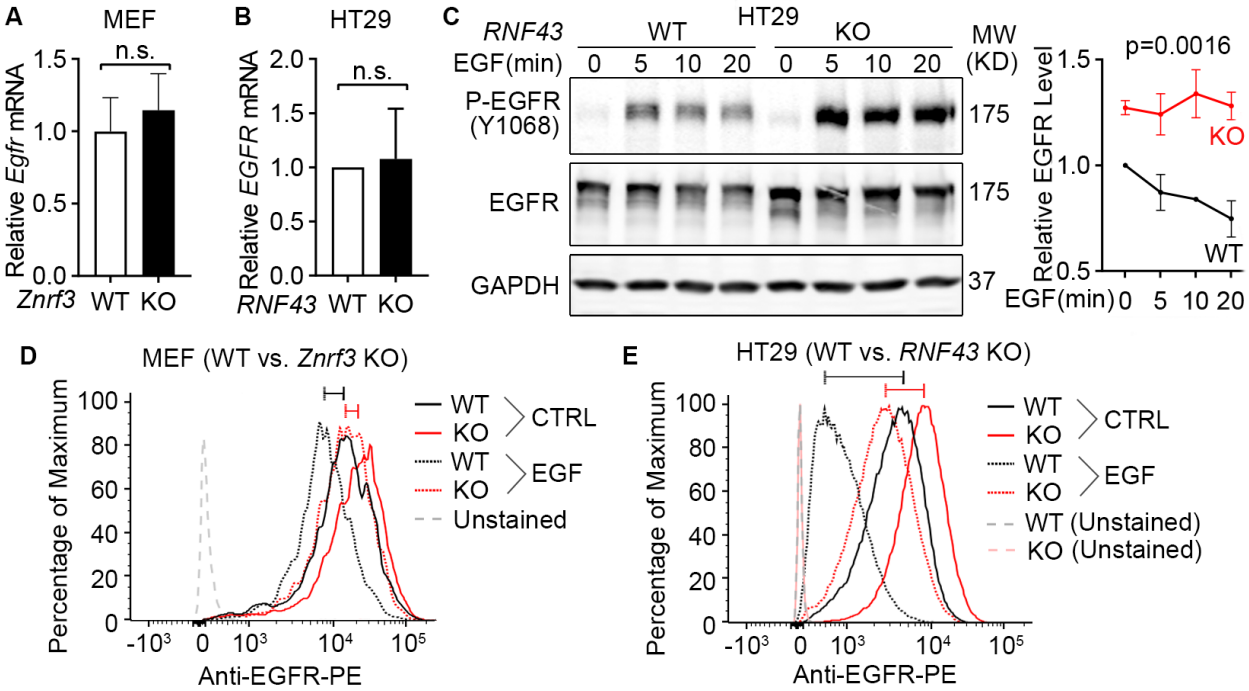
A
MEF
n.s.
Relative Egfr mRNA
1.5
1.0
0.5
0.0
Znrf3 WT KO
B
HT29
n.s.
Relative EGFR mRNA
2.0
1.5
1.0
0.5
0.0
RNF43 WT KO
C
RNF43
WT
HT29
KO
MW
EGF(min) 0 5 10 20 0 5 10 20
(KD)
P-EGFR
(Y1068)
175
EGFR
175
GAPDH
37
p=0.0016
Relative EGFR Level
1.5
1.0
0.5
KO
WT
EGF(min) 0 5 10 20
D
MEF (WT vs. Znrf3 KO)
Percentage of Maximum
100
80
60
40
20
0
-10³ 0 10³ 10⁴ 10⁵
Anti-EGFR-PE
WT
KO
CTRL
WT
KO
EGF
Unstained
E
HT29 (WT vs. RNF43 KO)
Percentage of Maximum
100
80
60
40
20
0
-10³ 0 10³ 10⁴ 10⁵
Anti-EGFR-PE
WT
KO
CTRL
WT
KO
EGF
WT (Unstained)
KO (Unstained)

962

963

964 Fig.3 Loss of ZNRF3/RNF43 delays EGFR protein degradation.

965 **A**. Knockout of *Znrf3* has no impact on *Egfr* mRNA level in MEFs.

966 **B**. Knockout of *RNF43* has no impact on *EGFR* mRNA level in HT29 cells.

967 **C**. *RNF43* knockout inhibits EGF-induced EGFR protein degradation in HT29 cells. Cells were
968 stimulated with EGF (50 ng/ml) for indicated times. Representative western blot images (left panel)
969 and quantification results (right panel) were shown.

970 **D**. *Znrf3* knockout increases the cell surface level of EGFR protein in MEFs unstimulated or
971 stimulated with EGF (50 ng/ml, 10 min).

972 **E**. *RNF43* knockout increases the cell surface level of EGFR protein in HT29 cells unstimulated
973 or stimulated with EGF (50 ng/ml, 10 min). The bars mark the relative peak shifts after EGF
974 stimulation in WT (black) or KO (red) cells.

975 Means ± SEMs are shown. *p*-values were calculated by Welch's t-test (**A**, **B**) or two-way ANOVA
976 uncorrected Fisher's LSD test (**C**). n.s., not significant.

977

978

979

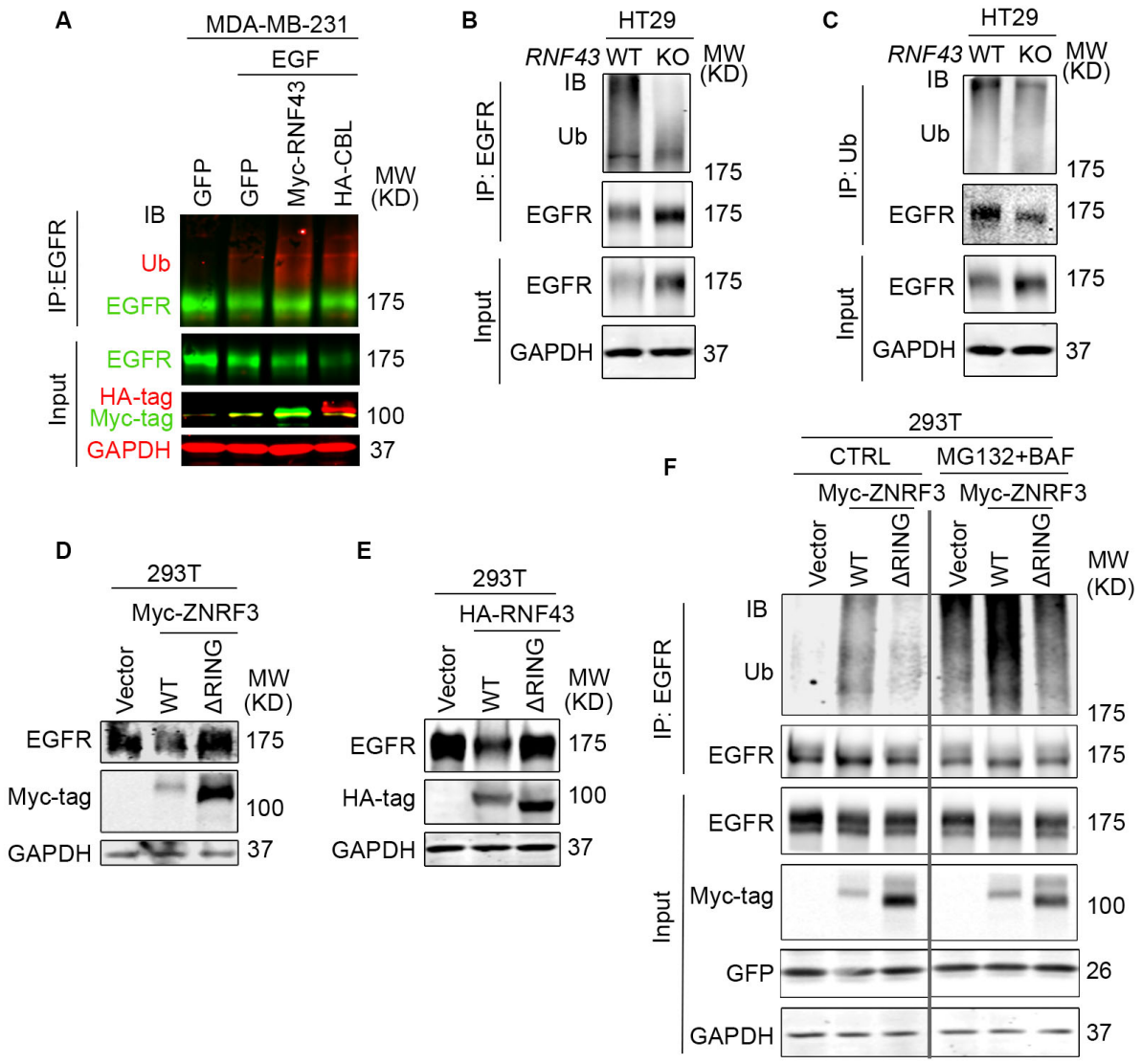
A
MDA-MB-231
EGF
GFP
GFP
Myc-RNF43
HA-CBL
MW (KD)
IP:EGFR
IB
Ub
EGFR
175
Input
EGFR
175
HA-tag
Myc-tag
100
GAPDH
37
B
HT29
RNF43 WT KO
MW (KD)
IP: EGFR
IB
Ub
175
EGFR
175
Input
EGFR
175
GAPDH
37
C
HT29
RNF43 WT KO
MW (KD)
IP: Ub
IB
Ub
175
EGFR
175
Input
EGFR
175
GAPDH
37
D
293T
Myc-ZNRF3
Vector
WT
ΔRING
MW (KD)
EGFR
175
Myc-tag
100
GAPDH
37
E
293T
HA-RNF43
Vector
WT
ΔRING
MW (KD)
EGFR
175
HA-tag
100
GAPDH
37
F
293T
CTRL
MG132+BAF
Myc-ZNRF3
Myc-ZNRF3
Vector
WT
ΔRING
Vector
WT
ΔRING
MW (KD)
IP: EGFR
IB
Ub
175
EGFR
175
Input
EGFR
175
Myc-tag
100
GFP
26
GAPDH
37

980

981

982 Fig.4 ZNRF3/RNF43 enhances EGFR ubiquitination through the RING domain

983 **A**. Overexpression of RNF43 enhances EGFR ubiquitination level upon EGF (50 ng/ml)
984 stimulation in MDA-MB-231 cells. CBL serves as a positive control. Cells were co-infected with
985 lentivirus expressing EGFR and GFP, RNF43, or CBL.

986 **B**, **C**. Knockout of *RNF43* decreases EGFR ubiquitination in HT29 cells. (**B**) EGFR ubiquitination
987 was examined by Ub IP followed by EGFR IB; (**C**) HT29 cells were pretreated with 20 μM MG132
988 and 100 nM Bafilomycin A1 for 4 hr. EGFR ubiquitination after EGF treatment (50 ng/ml, 30 min)
989 was examined by EGFR IP followed by Ub IB.

990 **D**, **E**. ZNRF3/RNF43 downregulates EGFR protein level through the RING domain. 293T cells
991 were co-transfected with EGFR and Vector, ZNRF3 WT or ΔRING mutant (**D**), RNF43 WT or
992 ΔRING mutant (**E**).

993 **F**. ZNRF3 regulates EGFR ubiquitination through the RING domain. 293T cells were co-
994 transfected with EGFR and Vector, ZNRF3 WT or ΔRING mutant. EGFR ubiquitination after
995 EGF treatment (50 ng/ml, 10 min) was examined by EGFR IP followed by Ub IB. Cells were
996 pretreated with 20 μM MG132 and 100 nM Bafilomycin A1 for 4 hr.

997

998

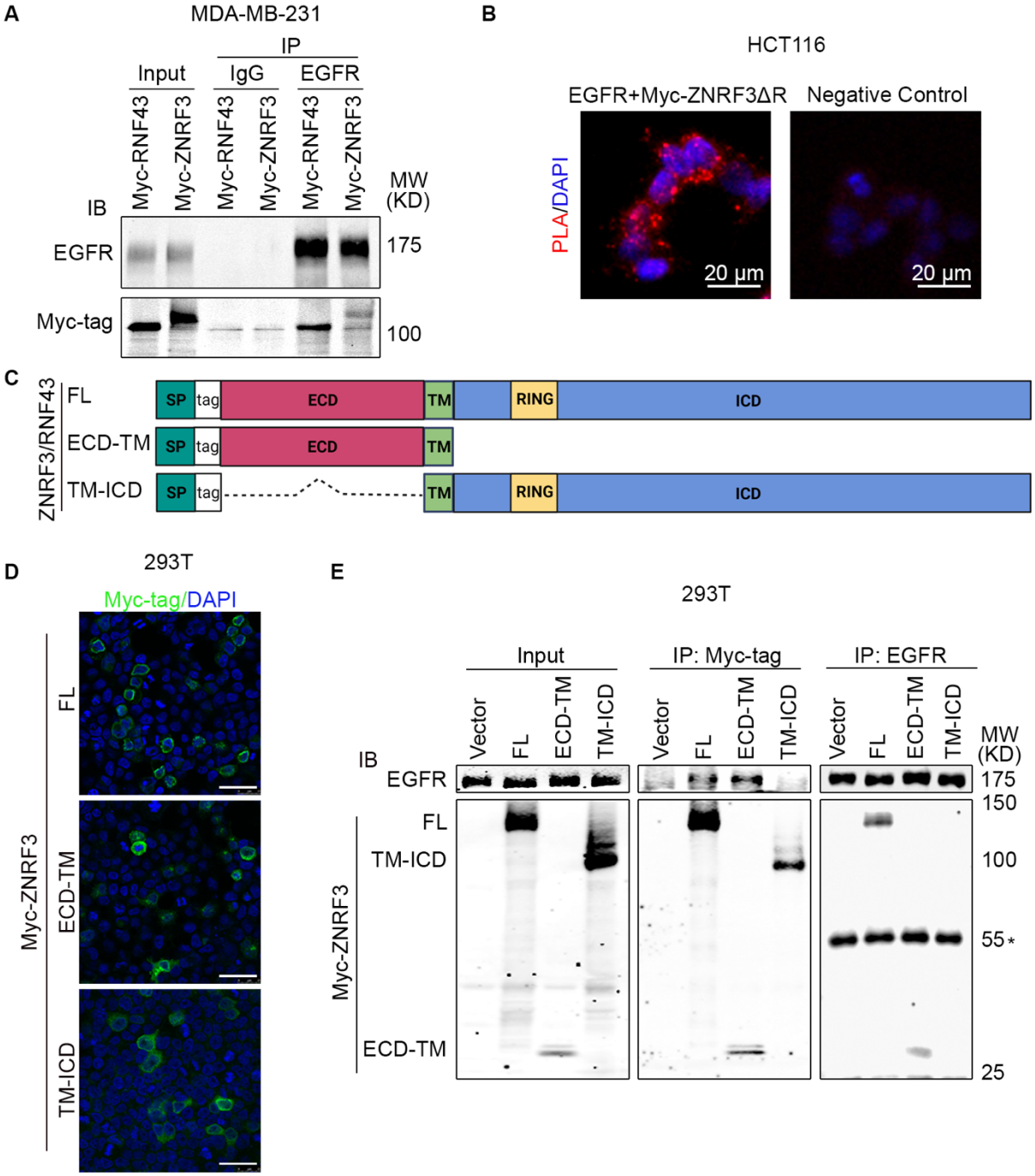
A
MDA-MB-231
IP
Input
IgG
EGFR
Myc-RNF43
Myc-ZNRF3
Myc-RNF43
Myc-ZNRF3
Myc-RNF43
Myc-ZNRF3
MW (KD)
IB
EGFR
175
Myc-tag
100
B
HCT116
EGFR+Myc-ZNRF3ΔR
Negative Control
PLA/DAPI
20 μm
20 μm
C
ZNRF3/RNF43
FL
ECD-TM
TM-ICD
SP
tag
ECD
TM
RING
ICD
D
293T
Myc-tag/DAPI
Myc-ZNRF3
FL
ECD-TM
TM-ICD
E
293T
Input
IP: Myc-tag
IP: EGFR
Vector
FL
ECD-TM
TM-ICD
MW (KD)
IB
EGFR
175
150
100
55*
25
Myc-ZNRF3
FL
TM-ICD
ECD-TM

1001 Fig. 5 ZNRF3/RNF43 interacts with EGFR through the extracellular domain

1002 **A**. Ectopically expressed EGFR is co-immunoprecipitated with Myc-tagged RNF43 and ZNRF3
1003 in MDA-MB-231 cells.

1004 **B**. Representative images of proximity ligation assay in HCT116 cells co-transfected with EGFR
1005 and Myc-ZNRF3ΔRING. Red, PLA signals; Blue, DAPI nuclei staining; Scale bar=20 μm.

1006 **C**. Schematic diagram of tagged ZNRF3/RNF43 proteins. SP, signal peptide; FL, full-length; ECD,
1007 extracellular domain; TM, transmembrane domain; ICD, intracellular domain; RING, E3 ligase
1008 RING domain.

1009 **D**. Immunofluorescence staining for ZNRF3 in 293T cells expressing Myc-tagged ZNRF3 FL,
1010 ECD-TM, TM-ICD. Scale bar=40 μm.

1011 **E**. ZNRF3 extracellular domain is required for ZNRF3 interaction with EGFR. 293T cells were
1012 co-transfected with EGFR and Myc-tagged ZNRF3 constructs and the lysate amounts were
1013 adjusted to achieve comparable levels of EGFR protein in each IP system (Input, left panel). EGFR
1014 interaction with ZNRF3 FL, ECD-TM, or TM-ICD were examined by Myc-tag IP followed by
1015 EGFR IB (middle panel) or by EGFR IP followed by Myc-tag IB (right panel). *, IgG heavy chain.

1016

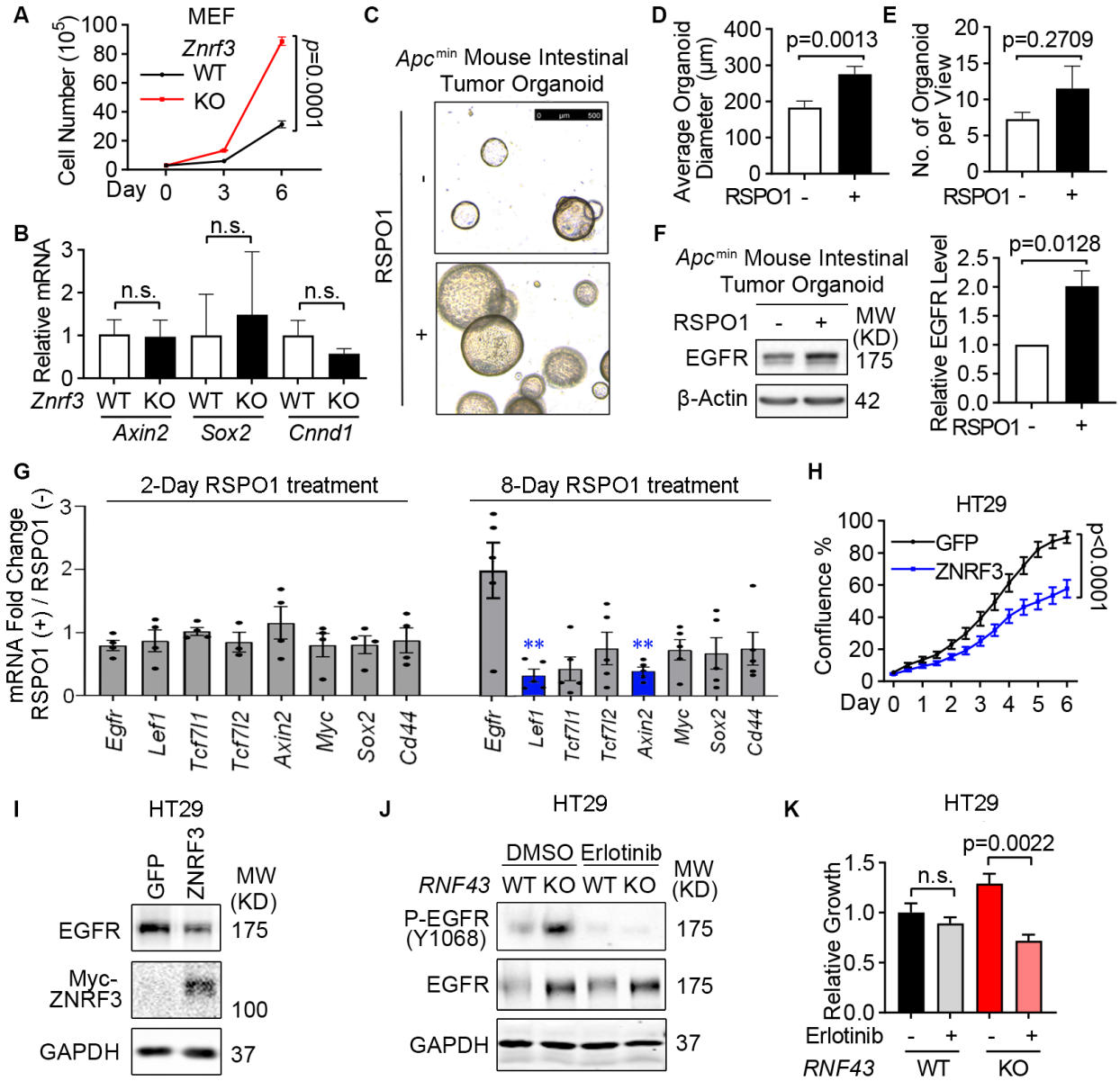

1017
1018

1019

1020 Fig. 6 ZNRF3/RNF43 inhibits EGFR-mediated cell growth

1021 **A**. Knockout of *Znrf3* enhances MEF cell growth, as measured by cell counting at the indicated
1022 time points.

1023 **B**. qPCR analysis for WNT target genes in WT and *Znrf3* KO MEFs.

1024 **C**-**E**. Supplementing RSPO1 promotes *Apc*^{min} mouse intestinal tumor organoid growth. The equal
1025 number of single cells from *Apc*^{min} mouse intestinal tumor organoids were embedded in Matrigel
1026 and cultured without or with 10% RSPO1 conditioned medium for 8 days. Representative images
1027 (**C**), and quantification of the size (**D**) and number (**E**) of formed *Apc*^{min} mouse intestinal tumor
1028 organoids are shown. Scale bar = 500 μm.

1029 **F**. Supplementing RSPO1 enhances EGFR protein level in *Apc*^{min} mouse intestinal tumor
1030 organoids. Representative images (left panel) and quantification (right panel) of EGFR protein
1031 level are shown.

1032 **G**. qPCR analysis for *Egfr* and WNT target genes in *Apc*^{min} mouse intestinal tumor organoids
1033 cultured with or without RSPO1 supplements. Genes with no significant changes after RSPO1
1034 treatment were plotted in grey, genes significantly down-regulated after RSPO1 treatment were
1035 plotted in blue. **, p-value < 0.01.

1036 **H**. Overexpression of ZNRF3 inhibits HT29 cell growth. HT29 cells stably overexpressing GFP
1037 or ZNRF3 were seeded in equal numbers and measured by confluence percentage using Incucyte.

1038 **I**. Overexpression of ZNRF3 reduces EGFR protein level in HT29 cells.

1039 **J**. Erlotinib treatment blocks EGFR phosphorylation in WT and *RNF43* KO HT29 cells. Cells
1040 were treated with 5 μM erlotinib for 48 hr.

1041 **K**. Erlotinib treatment inhibits cell growth in *RNF43* KO HT29 cells.

1042 Means ± SEMs are shown. p-values were calculated by two-way ANOVA uncorrected Fisher's
1043 LSD test (**A**, **H**), Welch's t-test (**B**, **D**-**G**), one-way ANOVA uncorrected Fisher's LSD test (**K**).
1044 n.s., not significant.

1045

1046

1047

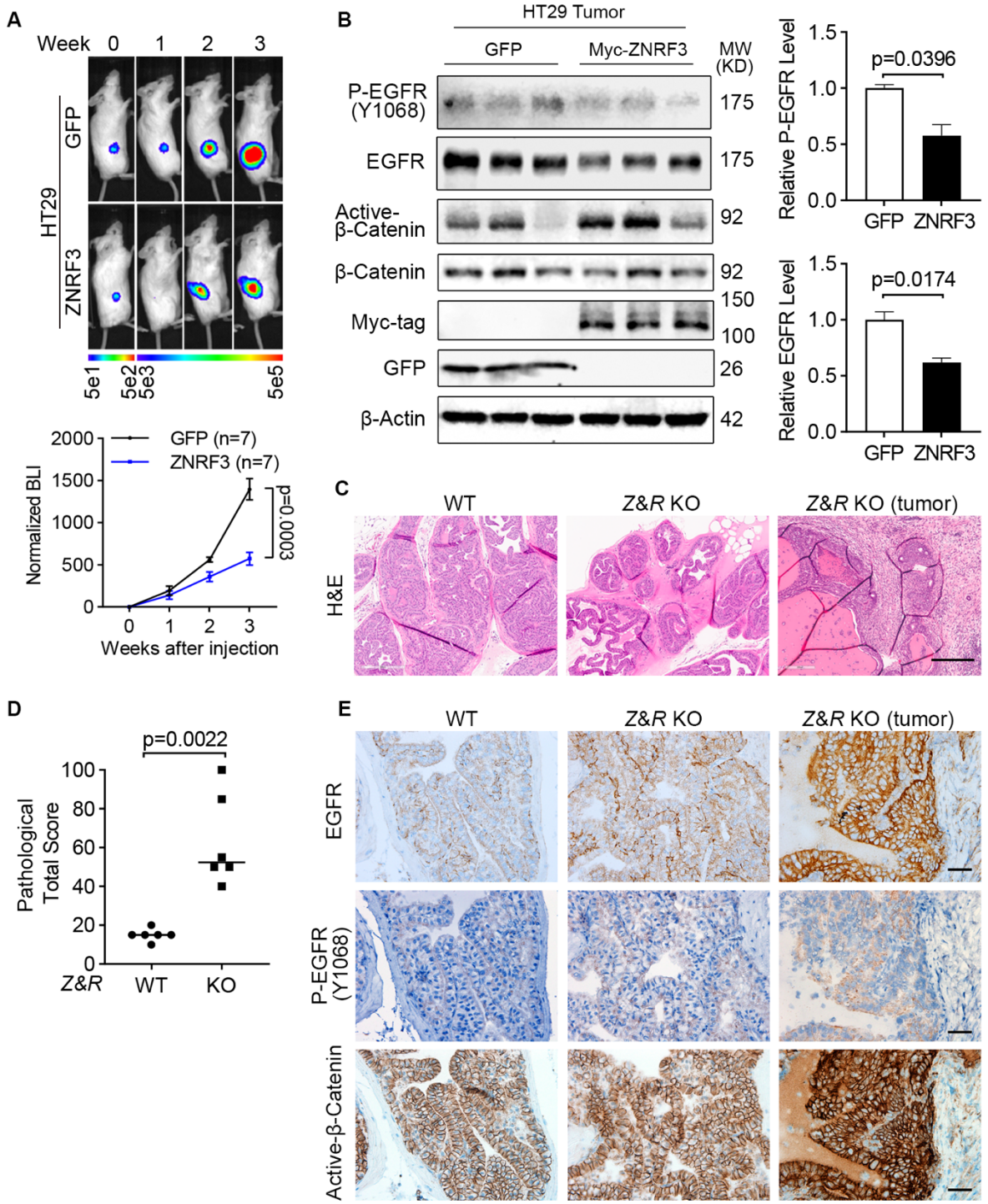
A
Week 0 1 2 3
HT29
GFP
ZNRF3
5e1 5e2 5e3 5e5
GFP (n=7)
ZNRF3 (n=7)
Normalized BLI
p=0.0003
Weeks after injection
B
HT29 Tumor
GFP
Myc-ZNRF3
MW (KD)
P-EGFR (Y1068)
EGFR
Active-β-Catenin
β-Catenin
Myc-tag
GFP
β-Actin
175
175
92
92
150
100
26
42
Relative P-EGFR Level
p=0.0396
Relative EGFR Level
p=0.0174
GFP ZNRF3
C
WT
Z&R KO
Z&R KO (tumor)
H&E
D
p=0.0022
Pathological Total Score
Z&R WT KO
E
WT
Z&R KO
Z&R KO (tumor)
EGFR
P-EGFR (Y1068)
Active-β-Catenin

1048

1049

1050 Fig. 7 ZNRF3/RNF43 loss enhances EGFR signaling and promotes tumorigenesis.

1051 **A**. Overexpression of ZNRF3 suppresses HT29 tumor growth *in vivo*. Representative
1052 bioluminescence images (top panel) and quantification (bottom panel) of flank-injected HT29 cells
1053 expressing either GFP or Myc-tagged ZNRF3.

1054 **B**. Overexpression of ZNRF3 inhibits P-EGFR and total EGFR levels in HT29 tumors.
1055 Representative images (left panel) and quantification of P-EGFR (right-top panel) and total EGFR
1056 (right-bottom panel) protein levels are shown.

1057 **C**. Representative H&E images of prostate tissues from WT or prostate-specific *Znrf3*/*Rnf43*
1058 knockout mice. Prostate tissue or tumor samples were collected at 1-year-old. Scale bar=300 μm.

1059 **D**. Total pathological scores of prostate tissues from WT or prostate-specific *Znrf3*/*Rnf43* knockout
1060 mice. n=6 mice per group.

1061 **E**. Representative images of immunochemistry staining for EGFR, P-EGFR, and active-β-Catenin
1062 in prostate tissues from WT or prostate-specific *Znrf3*/*Rnf43* knockout mice. Scale bar=40 μm.

1063 Means ± SEMs are shown. *p*-values were calculated by two-way ANOVA uncorrected Fisher's
1064 LSD test (**A**), Welch's t-test (**B**), Mann-Whitney (**D**).

1065

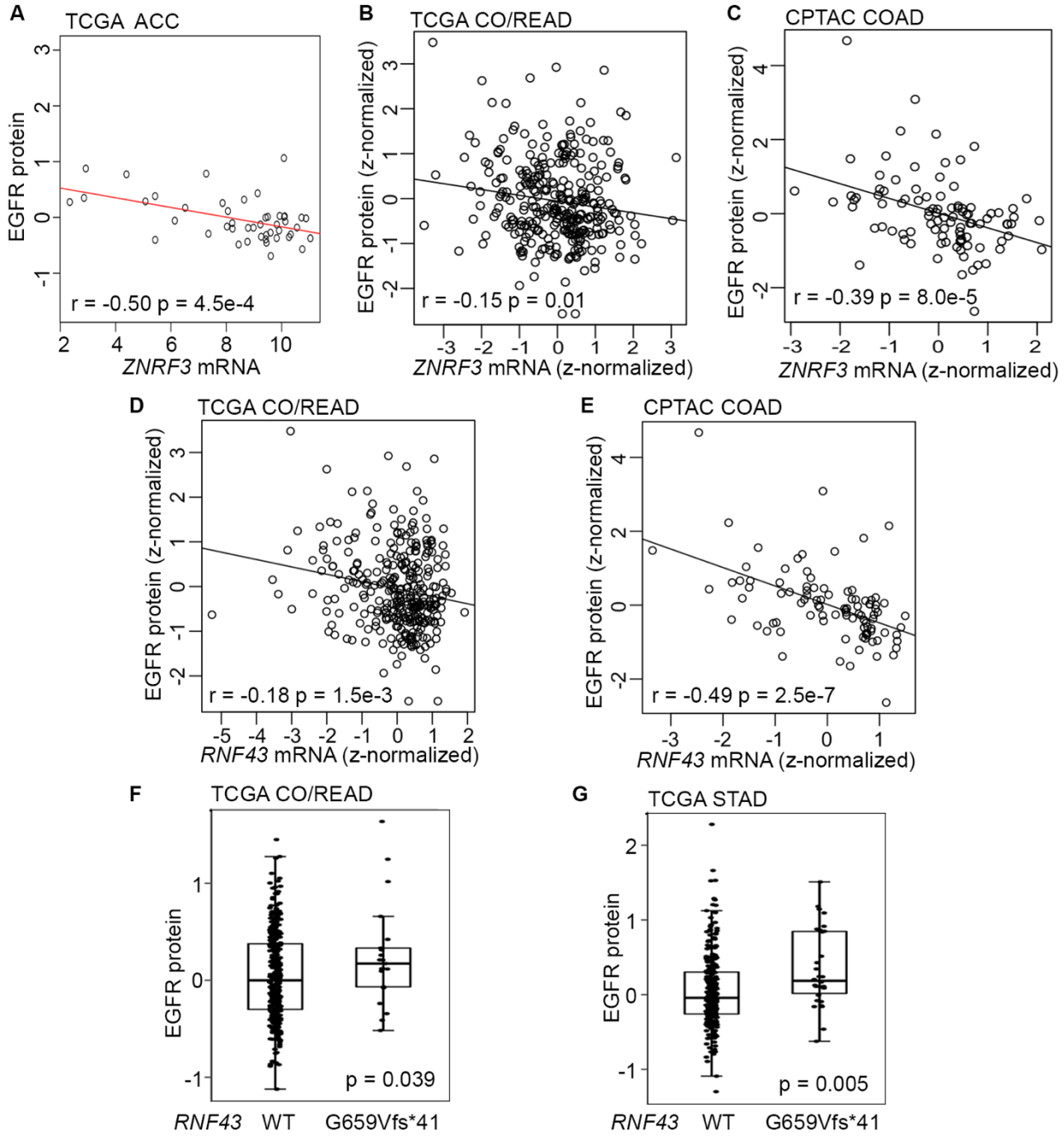
A
TCGA ACC
EGFR protein
ZNRF3 mRNA
r = -0.50 p = 4.5e-4
B
TCGA CO/READ
EGFR protein (z-normalized)
ZNRF3 mRNA (z-normalized)
r = -0.15 p = 0.01
C
CPTAC COAD
EGFR protein (z-normalized)
ZNRF3 mRNA (z-normalized)
r = -0.39 p = 8.0e-5
D
TCGA CO/READ
EGFR protein (z-normalized)
RNF43 mRNA (z-normalized)
r = -0.18 p = 1.5e-3
E
CPTAC COAD
EGFR protein (z-normalized)
RNF43 mRNA (z-normalized)
r = -0.49 p = 2.5e-7
F
TCGA CO/READ
EGFR protein
p = 0.039
RNF43 WT G659Vfs*41
G
TCGA STAD
EGFR protein
p = 0.005
RNF43 WT G659Vfs*41

1066

1067

1068 Fig. S1 EGFR protein level is negatively associated with *ZNRF3*/*RNF43* mRNA expression in
1069 cancers.
1070 **A**. Scatterplot of EGFR protein level (signal) versus *ZNRF3* mRNA expression (RSEM, Log2
1071 (Val+1)) using the TCGA adrenal cortical carcinoma (ACC) dataset.
1072 **B**. Scatterplot of EGFR protein level (z-normalized) versus *ZNRF3* mRNA expression (z-
1073 normalized) using the TCGA colorectal adenocarcinoma (CO/READ) dataset.
1074 **C**. Scatterplot of EGFR protein level (z-normalized) versus *ZNRF3* mRNA expression (z-
1075 normalized) using the CPTAC colon adenocarcinoma (COAD) dataset.
1076 **D**. Scatterplot of EGFR protein level (z-normalized) versus *RNF43* mRNA expression (z-
1077 normalized) using the TCGA colorectal adenocarcinoma (CO/READ) dataset.
1078 **E**. Scatterplot of EGFR protein level (z-normalized) versus *RNF43* mRNA expression (z-
1079 normalized) using the CPTAC colon adenocarcinoma (COAD) dataset.
1080 **F**. Boxplot of EGFR protein levels (signal) in human colorectal adenocarcinomas expressing
1081 RNF43 WT or RNF43 G659Vfs*41, using the TCGA dataset.
1082 **G**. Boxplot of EGFR protein levels (signal) in human stomach adenocarcinomas (STAD)
1083 expressing RNF43 WT or RNF43 G659Vfs*41, using the TCGA dataset.
1084

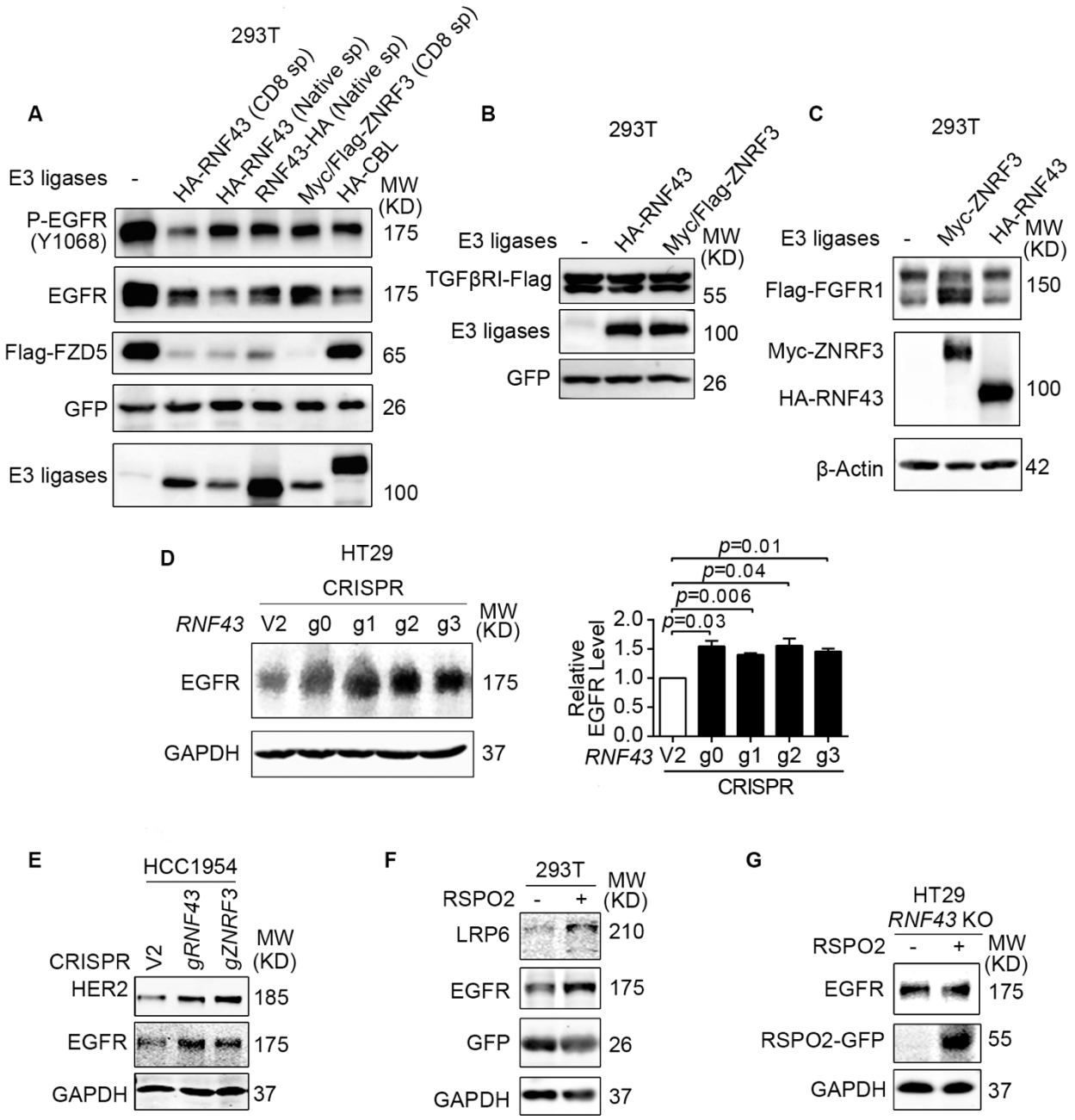
A
293T
E3 ligases
-
HA-RNF43 (CD8 sp)
HA-RNF43 (Native sp)
RNF43-HA (Native sp)
Myc/Flag-ZNRF3 (CD8 sp)
HA-CBL
MW (KD)
P-EGFR (Y1068)
175
EGFR
175
Flag-FZD5
65
GFP
26
E3 ligases
100
B
293T
E3 ligases
-
HA-RNF43
Myc/Flag-ZNRF3
MW (KD)
TGFβRI-Flag
55
E3 ligases
100
GFP
26
C
293T
E3 ligases
-
Myc-ZNRF3
HA-RNF43
MW (KD)
Flag-FGFR1
150
Myc-ZNRF3
HA-RNF43
100
β-Actin
42
D
HT29
CRISPR
RNF43
V2
g0
g1
g2
g3
MW (KD)
EGFR
175
GAPDH
37
p=0.01
p=0.04
p=0.006
p=0.03
Relative EGFR Level
2.0
1.5
1.0
0.5
0.0
RNF43
V2
g0
g1
g2
g3
CRISPR
E
HCC1954
CRISPR
V2
gRNF43
gZNRF3
MW (KD)
HER2
185
EGFR
175
GAPDH
37
F
293T
RSPO2
-
+
MW (KD)
LRP6
210
EGFR
175
GFP
26
GAPDH
37
G
HT29
RNF43 KO
RSPO2
-
+
MW (KD)
EGFR
175
RSPO2-GFP
55
GAPDH
37

1085

1086

1087 Fig. S2 ZNRF3/RNF43 negatively regulates EGFR protein level.

1088 **A**. Overexpression of RNF43 or ZNRF3 decreases P-EGFR, total EGFR, and FZD5 protein levels
1089 in 293T cells. GFP, EGFR, Flag-FZD5 constructs were co-transfected with E3 ligase constructs
1090 or vector control. CBL overexpression serves as a positive control for EGFR downregulation.
1091 RNF43 or ZNRF3 were expressed with their native signal peptides or CD8 signal peptide.

1092 **B**. Overexpression of RNF43 or ZNRF3 has no impact on TGF-β receptor I (TGFβRI) protein
1093 level in 293T cells. TGFβRI-Flag construct was co-transfected with RNF43, ZNRF3 or vector
1094 control.

1095 **C**. Overexpression of ZNRF3 or RNF43 does not decrease FGFR1 protein level in 293T cells.
1096 Flag-FGFR1 construct was co-transfected with ZNRF3, RNF43, or vector control.

1097 **D**. Expression of Cas9-CRISPR *RNF43* guide RNA enhances EGFR protein level in HT29 cells,
1098 shown by representative western blot images (left panel) and quantification results (right panel).

1099 **E**. Expression of Cas9-CRISPR *RNF43* guide RNA or *ZNRF3* guide RNA enhances both EGFR
1100 and HER2 protein levels in HCC1954 cells.

1101 **F**. RSPO2 treatment (50 ng/ml, 2-4 hr) enhances EGFR and LRP6 protein levels in 293T cells
1102 infected with lentivirus expressing FUCGW-EGFR.

1103 **G**. Overexpression of RSPO2 WT does not enhance EGFR protein level in HT29 *RNF43*
1104 knockout cells.

1105 Means ± SEMs are shown. *p*-values were calculated by one-way ANOVA uncorrected Fisher's
1106 LSD test. n.s., not significant.

1107

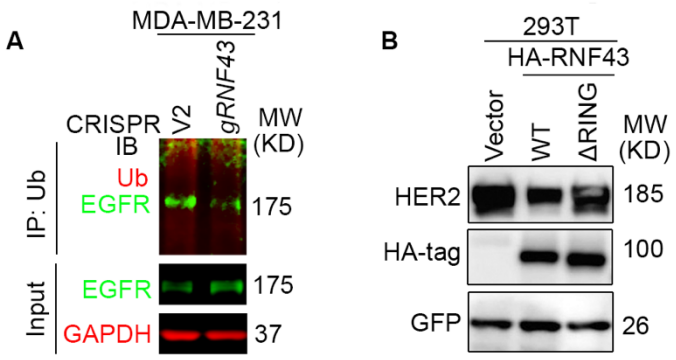

Fig. S3 RNF43 loss decreases EGFR ubiquitination.

A. Depletion of *RNF43* by CRISPR/Cas9 decreases EGFR ubiquitination in MDA-MB-231 cells. EGFR ubiquitination was examined by Ub IP followed by EGFR IB.

B. RNF43 downregulates HER2 protein level through the RING domain. 293T cells were co-transfected with HER2 and Vector, RNF43 WT or ΔRING mutant.

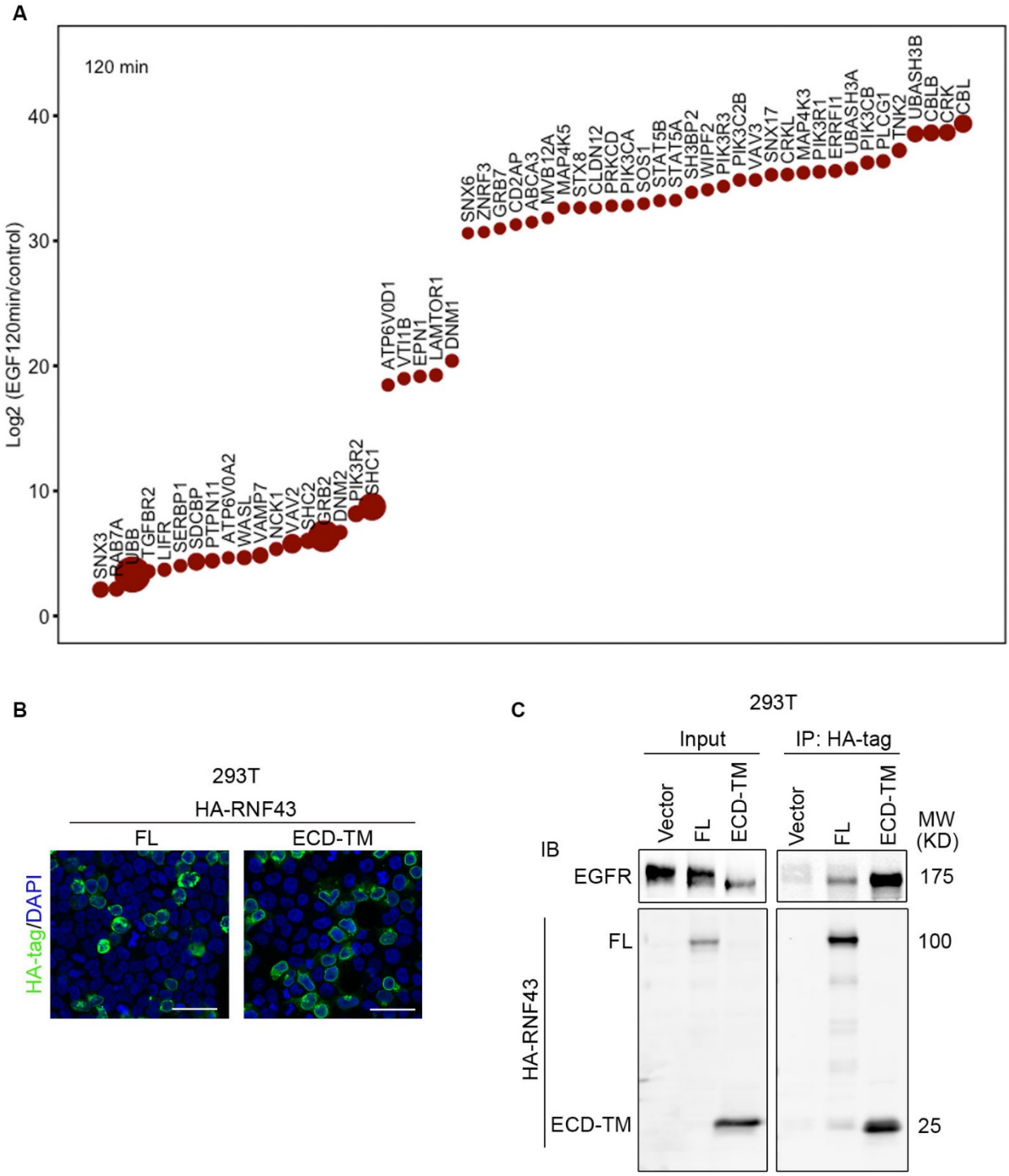

Fig. S4 ZNRF3/RNF43 interacts with EGFR

A. Relative abundance of the EGFR-associated proteins. BGC823 cells were starved overnight and then treated with 50 ng/ml EGF for 0 min (control) or 120 mins (EGF-stimulated). Endogenous EGFR was immunoprecipitated by anti-EGFR antibodies. EGFR-associated proteins with over

1121 10^5 iBAQ (intensity Based Absolute Quantification) and over 2-fold increase in iBAQ after EGF
1122 stimulation were plotted. The areas of the circles indicate the abundance of iBAQ of EGFR-
1123 associated proteins obtained in EGF-stimulated IPs. The y axis indicates the fold change of iBAQ
1124 of EGFR-associated proteins identified in EGF-stimulated versus control in the log2 scale, which
1125 are arranged from low to high along the x axis.
1126 **B**. Immunofluorescence staining for HA-tagged RNF43 FL and RNF43 ECD-TM in 293T cells
1127 transfected with RNF43 constructs. Scale bar=40 μm.
1128 **C**. RNF43 ECD-TM interacts with EGFR. 293T cells were co-transfected with EGFR and HA-
1129 tagged RNF43 constructs. EGFR interaction with RNF43 FL and RNF43 ECD-TM were examined
1130 by HA-tag IP followed by EGFR IB.
1131

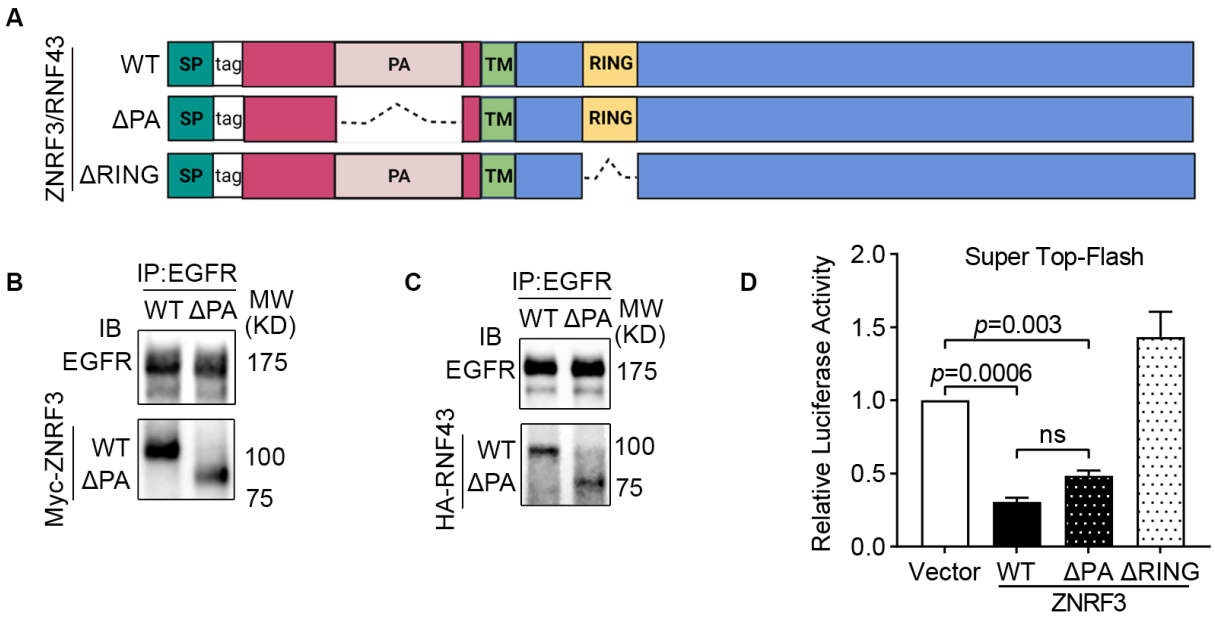

1132

1133 Fig. S5 The protease associate domain of ZNRF3/RNF43 is dispensable for EGFR interaction.

1134 **A**. Schematic diagram of tagged ZNRF3/RNF43 wild-type and mutant proteins. SP, signal peptide;

1135 WT, wild-type; PA, protease associate domain; TM, transmembrane domain; RING, E3 ligase

1136 RING domain.

1137 **B**, **C**. EGFR interacts with the ΔPA mutant of Myc-tagged ZNRF3 (**B**) and HA-tagged RNF43

1138 (**C**). 293T cells were co-transfected with EGFR and ZNRF3/RNF43 WT or ΔPA constructs.

1139 **D**. Overexpression of ZNRF3 WT or ΔPA mutant inhibits canonical WNT signaling in 293T cells

1140 in Super Top-Flash assay. ZNRF3 ΔRING mutant serves as a negative control.

1141 Means ± SEMs are shown. *p*-values were calculated by one-way ANOVA uncorrected Fisher's

1142 LSD test. n.s., not significant.

1143

1144

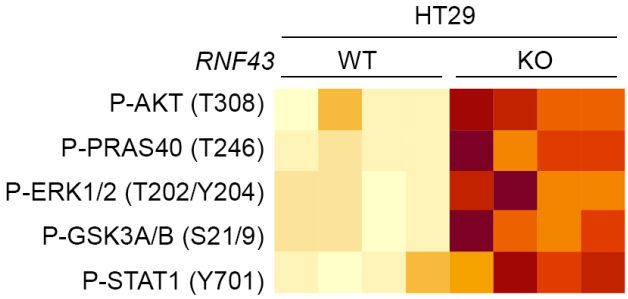

1145

1146 Fig. S6 RPPA identifies EGFR downstream signaling molecules upregulated by *RNF43* knockout

1147 in HT29 cells.

1148

1149

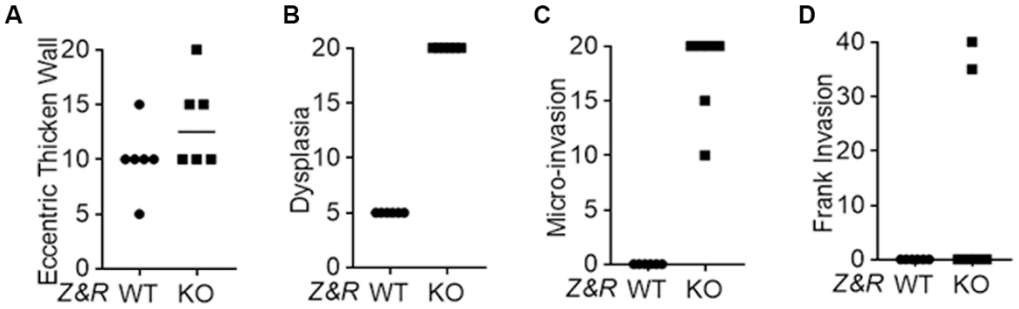

1150

1151 Fig. S7 Pathological assessment on eccentric thicken wall (A), dysplasia (B), micro-invasion (C),

1152 and frank invasion (D) of WT and *Znrf3*/*Rnf43* KO mouse prostate tissues.

1153
1154

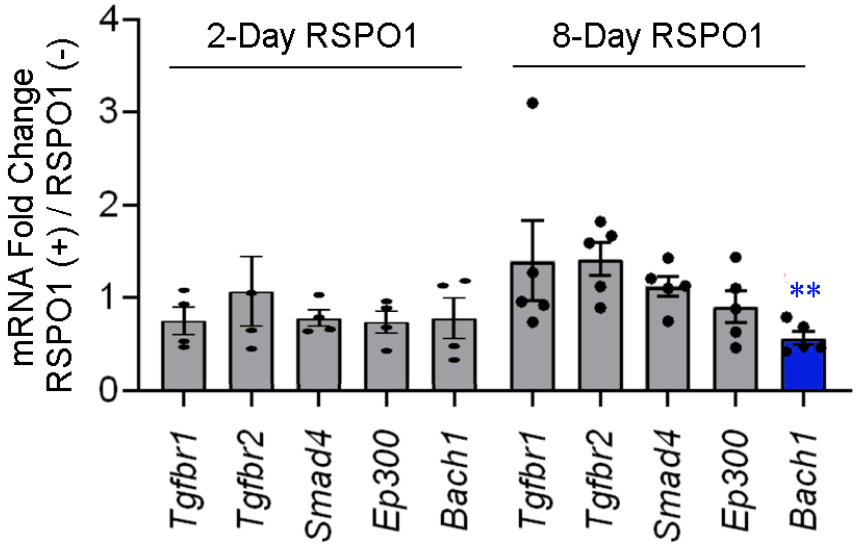

1155
1156 Fig. S8 qPCR analysis for TGF-β signaling relevant genes in *Apc*^{min} mouse intestinal tumor
1157 organoids cultured with or without RSPO1 supplements. Genes with no significant changes after
1158 RSPO1 treatment were plotted in grey, genes significantly down-regulated after RSPO1 treatment
1159 were plotted in blue. Means ± SEMs are shown. Welch's t-test was used to assess statistical
1160 significance. **, *p*-value < 0.01.
1161